ELSEVIER

Journal of Structural Geology 29 (2007) 1984–2005

JOURNAL OF STRUCTURAL GEOLOGY

www.elsevier.com/locate/jsg

Sustainable transpression: An examination of strain and kinematics in deforming zones with migrating boundaries

Dazhi Jiang [a,b,*]

[a] *Department of Earth Sciences, University of Western Ontario, London, ON, Canada N6A 5B7*
[b] *School of Resource and Environmental Engineering, Hefei University of Technology, Hefei, Anhui Province 230009, China*

Received 18 November 2006; received in revised form 6 September 2007; accepted 18 September 2007
Available online 2 October 2007

Abstract

Most orogenic belts owe their development to oblique convergence and commonly have many orogen-parallel transpressional high-strain zones. To constrain the tectonic history of orogenic belts by structural and fabric analysis of rocks, it is desirable to understand quantitatively the relationship between the boundary conditions and the resulting strain distribution and kinematics in these zones. Most current models for transpression assume homogeneous deformation confined by boundaries that are fixed to material planes. This creates a strain compatibility problem at the margins of the active deforming zone and also requires that the strain rate normal to the zone boundaries increase to implausibly high values soon after the onset of oblique convergence (transpressional motion). The latter contradicts with the observation that transpressional motion can be sustained throughout an orogeny. The assumption that zone boundaries are fixed to material planes is unrealistic. The outstanding problems of current transpressional models are resolved in this paper by allowing the zone boundaries to migrate through the rock material. The consequence of zone boundary migration for the strain field and kinematics within a transpressional high-strain zone is investigated mathematically. The implications of the modeling for fabric interpretation are discussed. The modeling makes general predictions consistent with observed planar and linear fabric patterns in natural transpressional high-strain zones. It predicts that foliations in transpressional high-strain zones are subparallel to the zone boundaries regardless of variation in the imposed boundary conditions. Lineations cluster along the great circle girdle subparallel to the average foliation. The spread of the lineations may vary from point maxima to complete girdles.

Keywords: Transpression; Oblique convergence; Shear zone; Modeling; Fabric; Lineation

1. Introduction

Most orogens, active convergent plate boundaries, and volcanic arcs are developed under oblique convergence between plates or blocks (e.g., Fitch, 1972; DeMets et al., 1990; McCaffrey, 1992, 1994) and host many orogen-parallel crustal scale fault systems in the brittle part of the lithosphere and high-strain zones in the ductile part of the lithosphere. Once established, a crustal scale fault and high-strain zone system can be active for a long time and exert a major control on the tectonic evolution of its hosting orogenic belt (e.g., Holdsworth et al., 1997; Tommasi and Vauchez, 2001; Ben-Zion and Sammis, 2003). These fault/high-strain zone systems collectively accommodate most of the relative motion between the bounding plates or blocks and commonly partition the overall oblique motion into more nearly thrust-like motions along shallowly- to moderately-dipping zones and more strike-slip-like motions along steeply-dipping to vertical zones (cf. Fitch, 1972; McCaffrey, 1992, 1994; Jones and Wesnousky, 1992; Bowman et al., 2003). Within each of these zones, the deformation is generally transpressional (Harland, 1971; Sanderson and Marchini, 1984), combining a boundary-normal shortening (thinning of Jiang and Williams, 1998) motion with a boundary-parallel simple shear motion. Because in general the simple shear component is not parallel to any of the

* Department of Earth Sciences, University of Western Ontario, London, ON, Canada N6A 5B7. Tel.: +519 661 3192; fax: +519 661 3198.
E-mail address: djiang3@uwo.ca

0191-8141/$ - see front matter © 2007 Elsevier Ltd. All rights reserved.
doi:10.1016/j.jsg.2007.09.007

principal directions of the thinning, pure shear component, the resulting deformation path in a transpressional zone within a plate-boundary region is generally triclinic (Jiang and Williams, 1998; Lin et al., 1998; Jiang et al., 2001). Studying the deformation history of crustal scale transpressional high-strain zones in orogenic belts may help to unravel the ancient slip partitioning across the belt and lead to better understanding of the responsible tectonic processes. Great efforts (see Jiang and Williams, 1998 and references therein) have been devoted to establishing the quantitative relationship between the boundary conditions of transpression and the strain geometry and kinematics within the deforming zone since McKenzie and Jackson (1983) and Sanderson and Marchini (1984), in recognition that this is the basis for using small-scale structural studies to reconstruct the deformation history of high-strain zones (e.g., Ramsay and Graham, 1970; Mattauer et al., 1981; Lister and Williams, 1983; Williams and Jiang, 2005). However, many fundamental problems remain unsolved, as discussed below.

1.1. Outstanding problems of transpression modeling

McKenzie and Jackson (1983) first used a continuum approach to relate the finite strain, palaeomagnetism, and fault movements within a deforming zone to the boundary movement conditions. Sanderson and Marchini (1984) investigated the finite strain inside a vertical tabular zone bounded by two obliquely converging rigid walls (Fig. 1a). In their model, the deformation in the zone is assumed homogeneous. A strain compatibility problem arises at the margins of the deforming zone because the rigid walls and the homogeneously deforming tabular zone must be separated by faults (Fig. 1a) unless the deforming zone is undergoing simple shear (e.g., Sanderson and Marchini, 1984; Schwerdtner, 1989; Robin and Cruden, 1994). Although Sanderson and Marchini's model has been extended to more general cases of monoclinic progressive deformation (Fossen and Tikoff, 1993; Tikoff and Fossen, 1993; Jones and Tanner, 1995; Jones et al., 1997) and triclinic progressive deformation (Jiang and Williams, 1998; Lin et al., 1998; Jiang et al., 2001; Jones et al., 2004), the strain compatibility problem remains not satisfactorily solved.

Robin and Cruden (1994) suggest a solution using heterogeneous strain across the deforming zone that maintains continuity with the rigid walls (Fig. 1b). Lin et al. (1998) assume that the bounding wall rocks undergo the same rate of pure shear as the deforming zone and therefore remain compatible with it. In this case, the deforming zone differs from the country rock only by its shear strain parallel to the zone boundary. However, neither proposal is without problem. The model of Robin and Cruden (1994) is based on Jaeger (1964, p. 140–142). The flow in the deforming zone is made of two components: one due to the zone boundaries approaching one another (the convergence component) and the other due to the boundary-parallel movement (the shear component). The convergence component causes an extrusional flow which, as Jaeger (1964, p. 140–142) shows, should cause a great tectonic overpressure (Robin and Cruden, 1994) at depth of the zone. There is no petrological evidence for such elevated pressure in any natural transpressional zones (cf. discussion in Williams et al., 2006). Further, this model predicts that foliations should be oblique to the zone boundaries near the margins of the zone (Robin and Cruden, 1994; Dutton, 1997). This is at odds with natural observations as well (Lin et al., 1998, 1999; Czeck and Hudleston, 2003, and this paper).

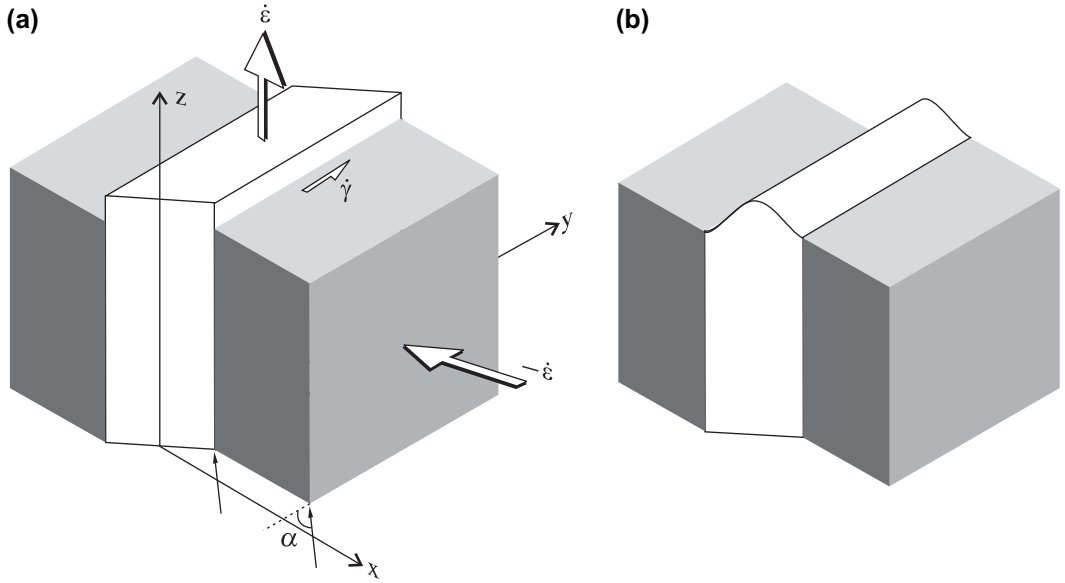

Fig. 1. (a) The transpression model of Sanderson and Marchini (1984) where the flow in the zone is homogeneous and monoclinic. The boundary-normal component of the convergence induces a pure shear strain rate ($\dot{\varepsilon}$) and the boundary-parallel component induces a simple shear strain rate ($\dot{\gamma}$) in the zone. The displacement is discontinuous across the zone boundaries between the deforming zone and the walls. (b) The model of Robin and Cruden (1994) in which the flow is heterogeneous across the zone and with depth. Displacement is continuous across the zone boundaries. For both models, the zone boundaries are fixed to material planes. *xyz*, The coordinate system used in this paper; α, convergence angle.

Lin et al. (1998, 1999) point out that the pure shear component of a high-strain zone is distributed over a much broader area than is the simple shear. To the first approximation, this may justify the assumption that the country rock has undergone the same rate of pure shear as the deforming zone. However, for a transpressional zone with a significant pure shear component, some degree of concentration of the rate of pure shear within the zone is likely. Allowing the pure shear strain rate to concentrate in the zone leads to another problem: the pure shear component acts to thin the zone (Jiang and Williams, 1998), which causes the pure shear strain rate, measured by vertical stretching ($\dot{\varepsilon}$), in the deforming zone, to increase rapidly with time according to $\dot{\varepsilon}(t) = \dot{\varepsilon}_0/(1 - \dot{\varepsilon}_0 \cdot t)$ (Appendix A), if the two blocks converge at a constant velocity ($\dot{\varepsilon}_0$ is the pure shear strain rate at the time of the onset of deformation) (Fig. 2a). Take a vertical transpressional zone with a convergence angle (α in Fig. 1a) of 30° for example. For a relative convergence velocity of 50 mm/year accommodated in a plate-boundary zone of 200 km wide (Schulmann et al., 2003), the pure shear strain rate would increase more than three orders of magnitude after some 8 million years of deformation (Fig. 2a). This would imply a phenomenal increase in stress in the zone unless the rocks weaken by the same orders of magnitude, which is in general unlikely. Alternatively, if the boundary condition is determined essentially by a constant stress (which, to the first approximation, is equivalent essentially to a constant strain rate $\dot{\varepsilon} \equiv \dot{\varepsilon}_0$), the boundary-normal velocity (V_n) must drop exponentially according to $V_n(t) = V_{n\,0} \cdot \exp(-\dot{\varepsilon}_0 \cdot t)$ (Appendix A) (V_{n0} is the initial velocity value at the onset of deformation) (Fig. 2b). Using the same example of a vertical transpressional zone with a convergence angle of 30°, the relative convergence velocity the zone can accommodate must drop to less than 30% of its initial value after some 10 million years of deformation if the pure shear strain rate in the zone is to remain constant. This would suggest that transpressional motion cannot be sustained for a long time, a conclusion contradictory to the observation that transpressional zones can last an entire orogeny of tens of million years or longer.

1.2. The patterns of linear fabrics in natural transpressional high-strain zones

In addition to the strain compatibility and motion sustainability problems, current transpression models cannot explain a repeatedly observed lineation pattern in natural transpressional zones. Natural transpressional zones have similar and simple planar fabrics. They have a dominant composite foliation which developed by transposition due to non-coaxial progressive deformation. This composite foliation is commonly defined by a compositional layering, which is typically of mixed origin, and is subparallel to the zone boundary. There may be another foliation defined by grain-shape fabric inclined to the transposition foliation. This is interpreted as an S-foliation (commonly a steady-state foliation of Means, 1981), in normal shear zone usage (Berthé et al., 1979). Lineations in natural transpressional high-strain zones are more variable in terms of geometrical patterns. They may form point maxima parallel to the shear direction or normal to the shear direction (e.g., Ramsay and Graham, 1970; Sanderson and Marchini, 1984; Tikoff and Greene, 1997), define half great circle girdles along the average foliation (Lin et al., 1998; Jiang et al., 2001; Lin and Jiang, 2001), or spread over the whole great circle subparallel to the zone boundary

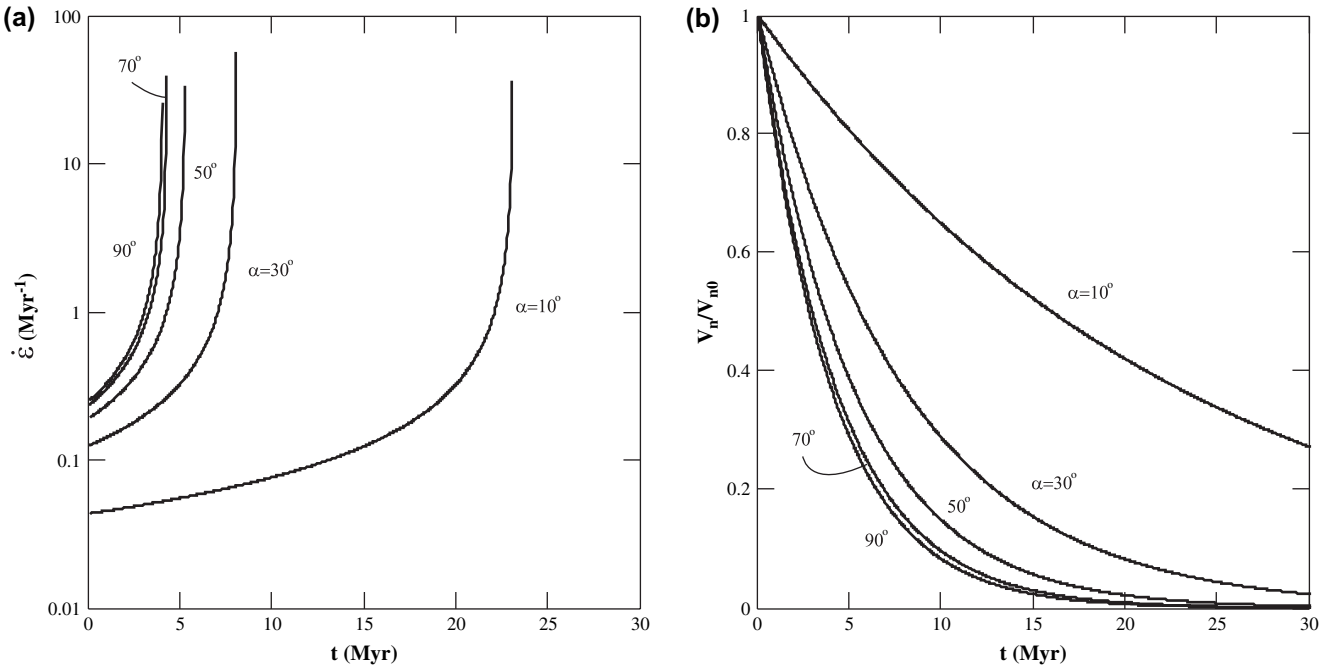

Fig. 2. The consequences of zone boundaries fixed to material planes. (a) The pure shear strain rate in the zone increases rapidly soon after the onset of transpressional motion if the convergence velocity is constant. (b) V_n, the boundary-normal component of the convergence velocity, must decrease exponentially if the strain rate in the zone remains constant. The curves are calculated based on an oblique convergence rate of 0.25 per million year, equivalent to that of a transpressional system of 200 km wide subjected to a relative convergence velocity of 50 mm/year. This convergence rate is used for all calculations in the paper.

(Czeck and Hudleston, 2003; Xu et al., 2003; Bentley, 2004). The whole great circle girdle pattern of lineation in natural transpressional high-strain zones is unexplained by any current models of transpressional zones.

1.3. A sustainable transpression model

Both the strain compatibility problem and motion sustainability problem can potentially be resolved by considering the migration of the deforming zone boundaries through rock material into hitherto undeformed country rocks (widening, in the sense of Means, 1995) so that the active deforming zone remains more or less a constant thickness to ensure a constant bulk strain rate for a constant boundary velocity. In this scenario, the wall rocks are fed into the deforming zone gradually and displacement continuity between the active deforming zone and the bounding blocks can be maintained throughout deformation. It is also of interest to investigate whether incorporating zone boundary migration into the model may generate the lineation pattern that spreads the whole great circle girdle along the average foliation as reported for many natural transpressional zones.

The concept of a deformation front migrating through rock material to maintain a roughly constant pure shear strain rate in the active deforming zone is not new (Ben-Avraham and Nur, 1976; Dewey et al., 1986). Dewey et al. (1986) estimate that the average pure shear strain rate for the Alpine/Himalayan convergent zone remains roughly 1.5×10^{-15} s^{-1}, although the convergence rate varies from 10 to 50 mm/year, and the width of the deforming zone, as defined by earthquake distribution, ranges from a few hundred to several thousand kilometers. White et al. (1980) suggest that, to accommodate a given imposed displacement rate, a critical volume of mylonite must develop and a shear zone will grow laterally until this is achieved. Means (1995) specifically discusses narrowing and widening shear zones. However, the consequence of boundary migration for the strain and kinematics in transpressional high-strain zones has not been generally investigated (see however Dutton, 1997).

In what follows, I investigate the strain geometry and kinematics of high-strain zones in which thinning of the zone (Jiang and Williams, 1998) is balanced by the outward migration of the zone boundaries (“widening” of Means, 1995). I am principally concerned with the variability of the finite strain geometry and kinematics of deformation, and its relationship with the boundary conditions. I will start with the simplest situation where the flow in the zone is homogeneous. To test the stability of the predictions of this simple model, I then consider a heterogeneous case where the simple shear strain rate in the zone varies. Finally, the model predictions are discussed in the context of natural data.

2. Mathematic description of transpression zones with migrating boundaries

Three different approaches have been used in strain and kinematics modeling of high-strain zones: the finite deformation approach (Ramsay and Graham, 1970; Sanderson and Marchini, 1984; Jones and Tanner, 1995; Jones et al., 1997, 2004, the steady-state incremental deformation approach (cf. Elliott, 1972; Fossen and Tikoff, 1993; Tikoff and Fossen, 1993), and the rate of deformation approach (cf. Ramberg, 1975; Jiang and Williams, 1998; Lin et al., 1998). The present paper uses the rate of deformation approach because it can handle both steady and non-steady progressive deformation readily and because the kinematic significance of deformation is the most explicit in this approach (Truesdell and Toupin, 1960, p. 349).

2.1. The homogeneous flow case

In the event the convergence velocity between bounding blocks is perfectly horizontal, there exists a horizontal plane called the “floor of transpression (FOT)” (Fig. 3a, b). The rock material above the FOT will move upward and that below the FOT will move downward unless the FOT is a detachment surface (cf. Royden, 1996; Schulmann et al., 2003; Little, 2004).

Fig. 3 shows the homogeneous flow case considered in this paper. It assumes (1) the active zone thickness is constant (thinning is balanced by widening), (2) the flow in the deforming zone is homogeneous and constant with time, and (3) the flow in the deforming zone is symmetric about the central plane of the zone. To describe this model mathematically, a right-handed coordinate system, xyz, is set up with its origin on the FOT and at the center of the zone, the x-axis perpendicular to the zone boundary, the y-axis parallel to the strike of the zone, and the z-axis parallel to the dip line and pointing upward (Fig. 3a, b). The following external variables are necessary to define the model:

D: half thickness of the zone,
V: half of the relative velocity between the bounding blocks,
α: convergence angle, the angle between the horizontal component of V and the strike of the zone, and
β: dip angle of the zone.

In terms of instantaneous flow, the model is reduced to the Sanderson and Marchini model when $\beta = 90^\circ$ and to the triclinic model of Lin et al. (1998) when $0 < \beta < 90^\circ$. However, even for these end-member cases the finite strain geometry of the current model is distinct from previous models because the migration of zone boundaries is considered.

If it is assumed that the relative velocity V is perfectly horizontal, the strain rates in the zone are, respectively:

$$\begin{aligned}
\dot{\varepsilon}_v &= \frac{V}{D} \\
\dot{\varepsilon}_v &= \frac{V \sin\alpha \sin\beta}{D} = \dot{\varepsilon}_v \sin\alpha \sin\beta \\
\dot{\gamma}_{ss} &= \frac{V \cos\alpha}{D} = \dot{\varepsilon}_v \cos\alpha = \dot{\varepsilon} \cot\alpha \csc\beta \\
\dot{\gamma}_{ds} &= \frac{V \sin\alpha \cos\beta}{D} = \dot{\varepsilon}_v \sin\alpha \cos\beta = \dot{\varepsilon} \cot\beta
\end{aligned} \tag{1}$$

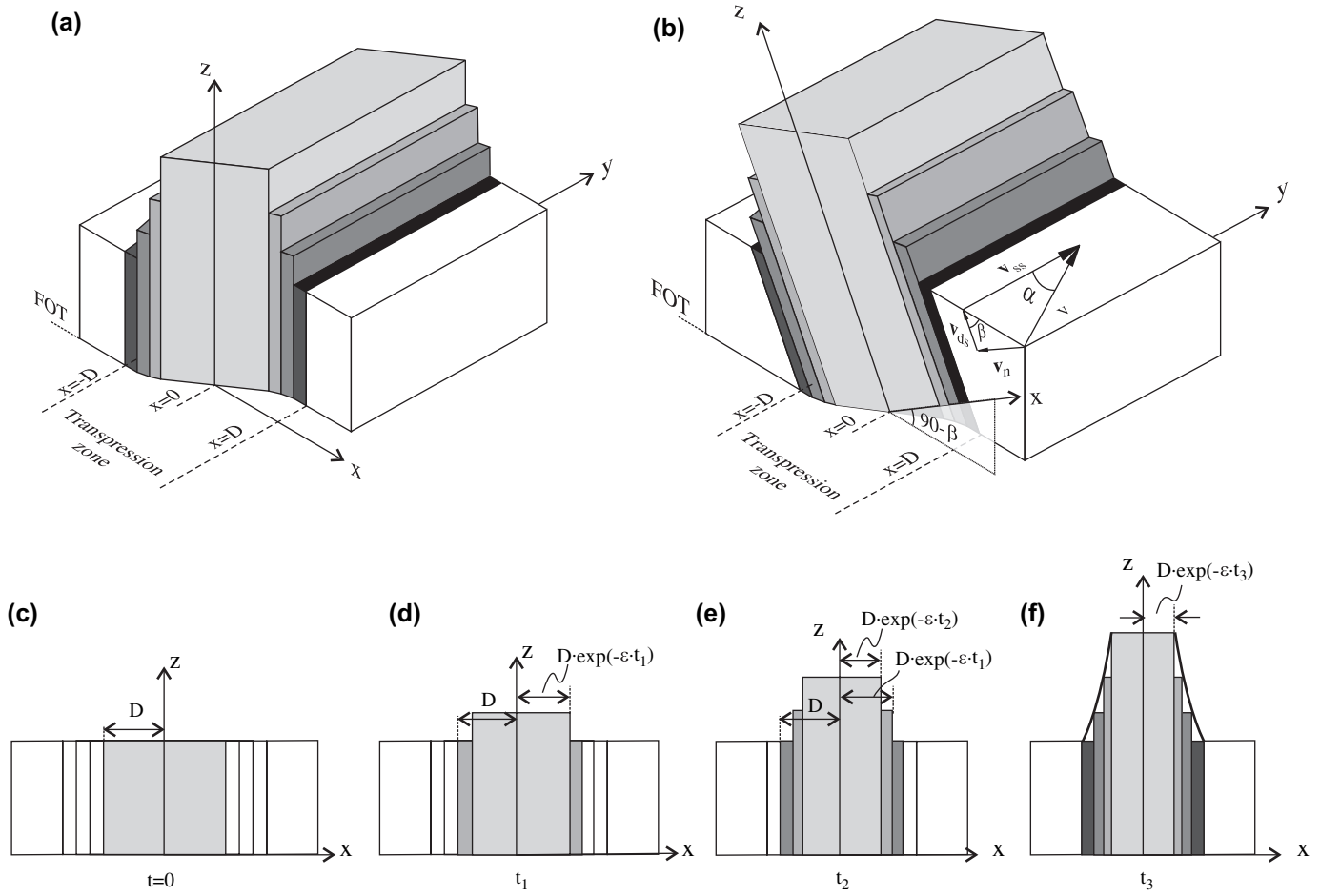

Fig. 3. Sustainable transpressional models with migrating zone boundaries investigated in this paper. (a) and (b) show, respectively, a vertical transpressional zone and an inclined (β, the dip angle) one. There is a horizontal plane, called the ''floor of transpression'' (FOT), which is either a decoupling plane (possible for both vertical and inclined transpression) or the plane of no shear stress for a vertical transpression zone. The deforming zone has a constant thickness throughout deformation when thinning is balanced by widening. (c)–(f) are cross sections for the vertical zone case schematically showing the progressive development. Even for the simplest situation where the flow in the zone is homogeneous, a strain gradient develops across the zone because the country rocks are fed into the zone progressively. There is no displacement discontinuity across the zone boundaries and no excess tectonic overpressures will build up at the depth of the zone.

where $\dot{\varepsilon}_v$, $\dot{\varepsilon}$, $\dot{\gamma}_{ss}$ and $\dot{\gamma}_{ds}$ are, respectively, called the oblique convergence rate, the pure shear strain rate, the strike-slip simple shear rate, and the dip-slip simple shear rate. If the relative velocity has a plunge angle ($\delta \neq 0°$, Fig. A1), the strain rates are related to boundary conditions by Eq. (A7) (Appendix B, Fig. A1). In the following, only the situation of $\delta = 0°$ is considered.

The Eulerian velocity field in the deforming zone is:

$$v_x = \frac{dx}{dt} = \begin{cases} -\dot{\varepsilon}x, & |x| \le D \\ -\dot{\varepsilon}D\cdot\mathrm{sign}(x), & |x| > D \end{cases} \tag{2a}$$

$$v_y = \frac{dy}{dt} = \begin{cases} \dot{\gamma}_{ss}x, & |x| \le D \\ \dot{\gamma}_{ss}D\cdot\mathrm{sign}(x), & |x| > D \end{cases} \tag{2b}$$

$$v_z = \frac{dz}{dt} = \begin{cases} \dot{\gamma}_{ds}x + \dot{\varepsilon}z, & |x| \le D \\ \dot{\gamma}_{ds}D\cdot\mathrm{sign}(x), & |x| > D \end{cases} \tag{2c}$$

where v_x, v_y, and v_z stand for the velocity components along respective coordinate axes.

Note that although the z-component of velocity is discontinuous at the zone boundaries ($|x| = D$) for z ≠ 0, the displacement is continuous there because of the advective effect that the wall rocks are fed into the active zone gradually. This will become clear when expressions for the displacements are obtained later (see Fig. 4).

Writing Eqs. (2) in coordinates normalized against D, we have:

$$v'_x = \frac{dx'}{dt} = \begin{cases} -\dot{\varepsilon}x', & |x'| \le 1 \\ -\dot{\varepsilon}\cdot\mathrm{sign}(x'), & |x'| > 1 \end{cases} \tag{3a}$$

$$v'_y = \frac{dy'}{dt} = \begin{cases} \dot{\gamma}_{ss}x', & |x'| \le 1 \\ \dot{\gamma}_{ss}\cdot\mathrm{sign}(x'), & |x'| > 1 \end{cases} \tag{3b}$$

$$v'_z = \frac{dz'}{dt} = \begin{cases} \dot{\gamma}_{ds}x' + \dot{\varepsilon}z', & |x'| \le 1 \\ \dot{\gamma}_{ds}\cdot\mathrm{sign}(x'), & |x'| > 1 \end{cases} \tag{3c}$$

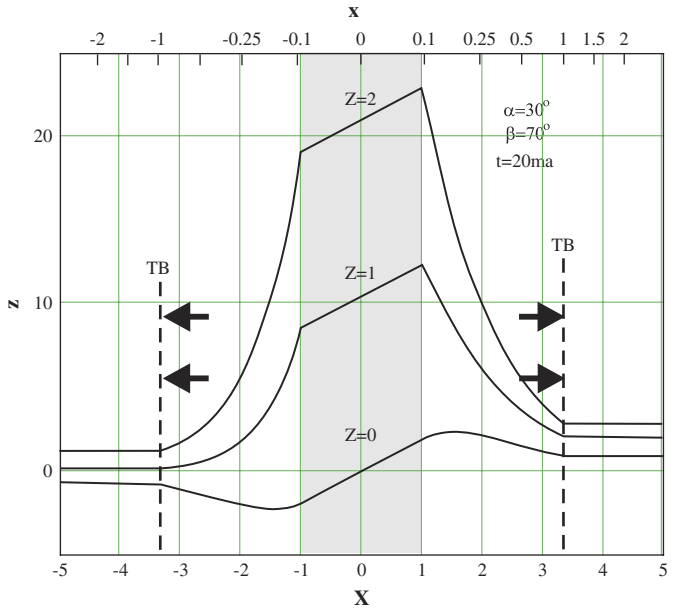

Fig. 4. A snapshot at $t = 20$ million year of the z-coordinates across the zone (against the horizontal Lagrangian coordinate X) for particles at initially different Z-values. TB marks the position of the current zone boundaries across which continuity is maintained. The corresponding Eulerian coordinate x is at the top of the diagram, and $x = \pm 1$ represents the active zone boundaries. Coordinates are all normalized against half thickness of the active zone.

where the primes stand for normalized coordinates (i.e., $x' = x/D$, $y' = y/D$, and $z' = z/D$). Only normalized coordinates are used hereafter and the prime signs are omitted.

$$y = \begin{cases} Y + \cot\alpha\,\csc\beta\, X(1 - \exp(-\dot{\varepsilon}t)), & \text{if } |X| \le 1 \quad \text{(i)} \\ Y + \cot\alpha\,\csc\beta(X - \operatorname{sign}(X)\exp(-\dot{\varepsilon}t + |X| - 1)), & \\ \qquad \text{if } |X| > 1 \text{ and } t > \xi \quad \text{(ii)} \\ Y + \operatorname{sign}(X)\dot{\varepsilon}\,\cot\alpha\,\csc\beta \cdot t, \quad \text{otherwise} \quad \text{(iii)} \end{cases} \tag{4b}$$

$$z = \begin{cases} Z\exp(\dot{\varepsilon}t) + X\cot\beta\,\sinh(\dot{\varepsilon}t), & \text{if } |X| \le 1 \quad \text{(i)} \\ (Z + X\cot\beta)\exp(\dot{\varepsilon}t - |X| + 1) - \cot\beta\,\cosh(\dot{\varepsilon}t - |X| + 1), & \\ \qquad \text{if } |X| > 1 \text{ and } t > \xi \quad \text{(ii)} \\ Z + \operatorname{sign}(X)\dot{\varepsilon}t\cot\beta, \quad \text{otherwise} \quad \text{(iii)} \end{cases} \tag{4c}$$

In Eqs. (4) and the following equations, $\xi = (|X| - 1)/\dot{\varepsilon}$ (see Eq. (A9) in Appendix C).

Eqs. (4a-i), (4b-i), and (4c-i) are for materials that have been involved in deformation since the onset of deformation (the central domain). Eqs. (4a-ii), (4b-ii), and (4c-ii) are for materials in 'the marginal domain' that were initially (at $t = 0$) outside of the deforming zone but were inside the zone at time t. Eqs. (4a-iii), (4b-iii), and (4c-iii) describe the (rigid-body) motion for materials that remain outside of the zone throughout deformation.

One can now use any equation from the set of Eqs. (4) to verify that continuity in displacement is maintained at the zone boundaries ($x = \pm 1$) throughout deformation (Fig. 4).

From Eqs. (4), the position gradient tensor $\mathbf{F}$(x, z, t) (with components: $F_{ij} = \partial x_i/\partial X_j$ where $i, j = 1, 2, 3$) for different domains can be obtained as follows:

$$F(x,z,t) = \begin{cases} \begin{pmatrix} \exp(-\dot{\varepsilon}t) & 0 & 0 \\ \cot\alpha\,\csc\beta(1 - \exp(-\dot{\varepsilon}t)) & 1 & 0 \\ \cot\beta\,\sinh(\dot{\varepsilon}t) & 0 & \exp(\dot{\varepsilon}t) \end{pmatrix}, & \text{if } |x| \le \exp(-\dot{\varepsilon}t), \text{ (central domain)} \quad \text{(a)} \\ \begin{pmatrix} |x| & 0 & 0 \\ \cot\alpha\,\csc\beta(1 - |x|) & 1 & 0 \\ -\operatorname{sign}(x)z + \cot\beta\left(\frac{1}{x} - x\right) & 0 & \frac{1}{|x|} \end{pmatrix}, & \text{if } \exp(-\dot{\varepsilon}t) < |x| \le 1, \text{ (marginal domain)} \quad \text{(b)} \\ \begin{pmatrix} 1 & 0 & 0 \\ 0 & 1 & 0 \\ 0 & 0 & 1 \end{pmatrix}, & \text{otherwise (wall rocks)} \quad \text{(c)} \end{cases} \tag{5}$$

Solving Eqs. (3) (Appendix C) yields the relationship between the Eulerian coordinates (x, y, z: the current position of a material particle at time t) and the Lagrangian coordinates (X, Y, Z: the initial position of the same material particle at $t = 0$) as follows:

$$x = \begin{cases} X\exp(-\dot{\varepsilon}t), & \text{if } |X| \le 1 \quad \text{(i)} \\ \operatorname{sign}(X)\exp(-\dot{\varepsilon}t + |X| - 1), & \\ \qquad \text{if } |X| > 1 \text{ and } t > \xi \quad \text{(ii)} \\ X - \operatorname{sign}(X)\dot{\varepsilon}t, \quad \text{otherwise} \quad \text{(iii)} \end{cases} \tag{4a}$$

2.2. The simple shear concentration case

If the simple shear components ($\dot{\gamma}_{ss}$, and $\dot{\gamma}_{ds}$) vary with x, the Eulerian and Lagrangian coordinates are related by (Appendix D):

$$x = \begin{cases} X\exp(-\dot{\varepsilon}t), & \text{if } |X| \le 1 \quad \text{(i)} \\ \operatorname{sign}(X)\exp(-\dot{\varepsilon}t + |X| - 1), & \\ \qquad \text{if } |X| > 1 \text{ and } t > \xi \quad \text{(ii)} \\ X - \operatorname{sign}(X)\dot{\varepsilon}t, \quad \text{otherwise} \quad \text{(iii)} \end{cases} \tag{6a}$$

$$y=\begin{cases} Y+\int_0^t\left(\int_0^x \dot{\gamma}_{ss}(x)\mathrm{d}x\right)\mathrm{d}t, \text{ if } |X|\le 1 & \text{(i)}\\ Y+\cot\alpha\csc\beta(X\cdot\mathrm{sign}(X)-1)+\int_\xi^t\left(\int_0^x \dot{\gamma}_{ss}(x)\mathrm{d}x\right)\mathrm{d}t, & \\ \quad \text{if } |X|>1 \text{ and } t>\xi & \text{(ii)}\\ Y+\mathrm{sign}(X)\dot{\varepsilon}\cot\alpha\csc\beta\cdot t, \text{ otherwise} & \text{(iii)}\end{cases} \tag{6b}$$

$$z=\begin{cases} \exp(\dot{\varepsilon}t)\left(Z+\int_0^t\left(\int_0^x \dot{\gamma}_{ds}(x)\mathrm{d}x\right)\exp(-\dot{\varepsilon}t)\mathrm{d}t\right), & \\ \quad \text{if } |X|\le 1 & \text{(i)}\\ \exp(\dot{\varepsilon}t)\left(Z+X-\mathrm{sign}(X)+\int_\xi^t\left(\int_0^x \dot{\gamma}_{ds}(x)\mathrm{d}x\right)\right. & \\ \qquad \left.\exp(-\dot{\varepsilon}t)\mathrm{d}t\right), \quad \text{if } |X|>1 \text{ and } t>\xi & \text{(ii)}\\ Z+\mathrm{sign}(X)\dot{\varepsilon}t\cot\beta, \quad \text{otherwise} & \text{(iii)}\end{cases} \tag{6c}$$

To obtain analytical expressions for the integral terms in the equation set, consider a special heterogeneous case in which the simple shear components are of the forms:

$$\begin{aligned}\dot{\gamma}_{ss}(x)&=\tfrac{\pi}{2}\dot{\varepsilon}\cot\alpha\csc\beta\cos\left(\tfrac{\pi}{2}x\right)\\ \dot{\gamma}_{ds}(x)&=\tfrac{\pi}{2}\dot{\varepsilon}\cot\beta\cos\left(\tfrac{\pi}{2}x\right)\end{aligned} \tag{7}$$

Eqs. (7) describe a situation where the simple shear strain rates reach their maxima ($(\pi/2)\dot{\varepsilon}\cot\alpha\csc\beta$ and $(\pi/2)\dot{\varepsilon}\cot\beta$, respectively) at the center of the zone ($x=0$) and drop to zero at the margins ($x=\pm1$). The particular forms of Eqs. (7) are chosen because they yield the average simple shear rates across the zone equal to the imposed values ($\dot{\varepsilon}\cot\alpha\csc\beta$ and $\dot{\varepsilon}\cot\beta$ for $\dot{\gamma}_{ss}$ and $\dot{\gamma}_{ds}$, respectively). Inserting Eqs. (7) into Eqs. (6), taking $F_{ij}=(\partial x_i/\partial X_j)$, and making use of the identity $\lim_{x\to 0}(\sin x/x)=1$, the position gradient tensor is obtained as follows:

3. Finite strain patterns

With Eqs. (5) and (8), it is possible to investigate the evolution of the finite strain field across the zone and with depth for any given set of external variables, that is, to relate the strain field within the deforming zone with the boundary conditions of transpression. The finite strain can be calculated by taking the eigenvalues and eigenvectors of the 'left Cauchy–Green tensor', **C**, which can be constructed from the position gradient tensor **F** (Truesdell and Toupin, 1960; Spencer, 1980). Written as a function of position and time, **C** is:

$$\mathbf{C}(x,z,t)=\mathbf{F}(x,z,t)\cdot\mathbf{F}(x,z,t)^{\mathrm{T}} \tag{9}$$

The eigenvalues of **C** are the magnitudes of the three principal quadric stretches (λ_1, λ_2, and λ_3) of the finite strains whereas their corresponding eigenvectors are the principal axes' orientations in the deformed state.

In the following, all computations are carried out with MathCad, a commercial software by Mathsoft Engineering &

$$\mathbf{F}(x,z,t)=\begin{cases} \begin{pmatrix} \exp(-\dot{\varepsilon}t) & 0 & 0\\ \frac{\pi}{2}\cot\alpha\csc\beta(1-\exp(-\dot{\varepsilon}t)) & 1 & 0\\ \frac{\pi}{2}\cot\beta\sinh(\dot{\varepsilon}t) & 0 & \exp(\dot{\varepsilon}t)\end{pmatrix}, \quad \text{if } x=0 & \\ \begin{pmatrix} \exp(-\dot{\varepsilon}t) & 0 & 0\\ \frac{\cot\alpha\csc\beta}{x\exp(\dot{\varepsilon}t)}\left(\sin\left(\frac{\pi}{2}x\exp(\dot{\varepsilon}t)\right)-\sin\left(\frac{\pi}{2}x\right)\right) & 1 & 0\\ \frac{2\cot\beta}{\pi}\left(\frac{\pi}{2}\left(\frac{\sin\left(\frac{\pi}{2}x\exp(\dot{\varepsilon}t)\right)}{x}-\frac{\sin\left(\frac{\pi}{2}x\right)}{x\exp(\dot{\varepsilon}t)}\right)+\frac{\cos\left(\frac{\pi}{2}x\exp(\dot{\varepsilon}t)\right)-\cos\left(\frac{\pi}{2}x\right)}{x^2\exp(\dot{\varepsilon}t)}\right) & 0 & \exp(\dot{\varepsilon}t)\end{pmatrix}, & \\ \qquad \text{if } |x|\le\exp(-\dot{\varepsilon}t) \text{ and } x\neq 0 & \\ \begin{pmatrix} x\cdot\mathrm{sign}(x) & 0 & 0\\ \cot\alpha\csc\beta\left(1-\sin\left(\frac{\pi}{2}x\right)\mathrm{sign}(x)\right) & 1 & 0\\ -\mathrm{sign}(x)\cdot z+x\cdot\cot\beta\cdot\mathrm{sign}(x)\left(1-x\cdot\sin\left(\frac{\pi}{2}x\right)\right) & 0 & \frac{1}{x\cdot\mathrm{sign}(x)}\end{pmatrix}, \quad \text{if } \exp(-\dot{\varepsilon}t)<|x|\le 1 & \\ \begin{pmatrix} 1 & 0 & 0\\ 0 & 1 & 0\\ 0 & 0 & 1\end{pmatrix}, \quad \text{otherwise} & \end{cases} \tag{8}$$

Education, Inc. (2002). Like in Fig. 2, the strain rates are based on a convergence rate $\dot{\varepsilon}_v = 7.93 \times 10^{-15}$ s^{-1} or 0.25 Myr^{-1}, equivalent to a transpressional belt of 200 km wide subjected to a relative convergence velocity of 50 mm/year. It should be noted that since only the strain geometry and kinematics are concerned, it does not matter what rate one uses; a faster rate enables the system to reach a certain strain state sooner, but does not change the strain geometry or kinematics.

3.1. The shape of finite strain ellipsoid

Figs. 5 and 6 present the Flinn diagrams of the finite strain evolution following material particles for the homogeneous flow case and the simple shear concentration case, respectively. For the homogeneous flow case (Fig. 5), if $\beta = 90°$ the evolution paths for particles in the central domain ($|X| < 1$) or on the FOT ($Z = 0$) are like those for homogeneous monoclinic transpression (Fossen and Tikoff, 1993; Tikoff and Fossen, 1993; Tikoff and Teyssier, 1994; Dewey et al., 1998). The Flinn curves for $\alpha < 19.5°$ ($\alpha = 10°$ is shown in Figs. 5a, 6a, b) are characterized by their bouncing off the abscissa. The Flinn curves for $\alpha > 19.5°$ are monotonic. In the marginal domain the bouncing off does not occur (Fig. 5b). The bouncing off is missing everywhere if $\beta \neq 90°$ (Fig. 5c, d).

All statements made above for the homogeneous flow case are also appropriate for the simple shear concentration case (Fig. 6). The bouncing off of the path curves only occurs in

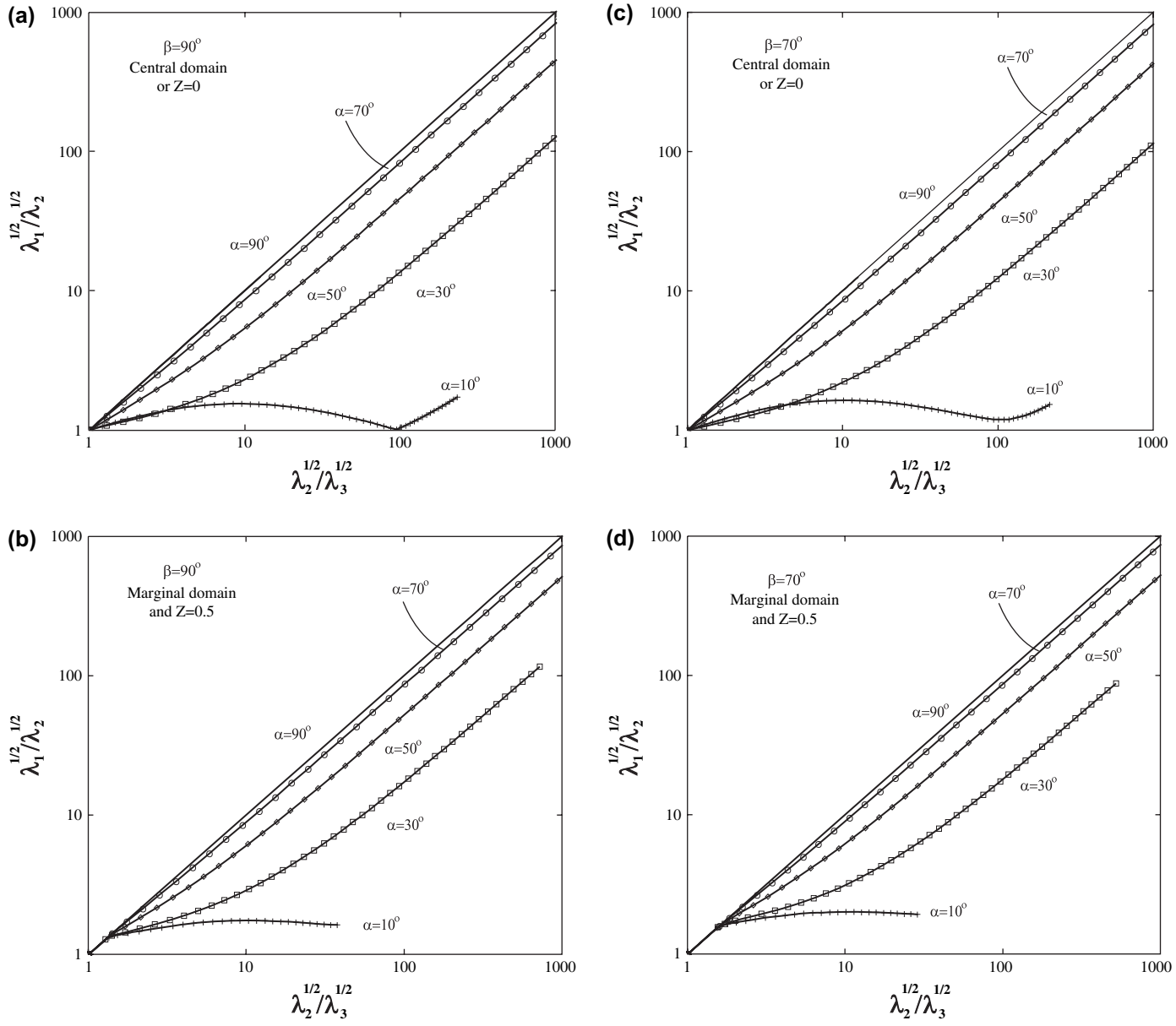

Fig. 5. Flinn diagrams showing evolution paths of the finite strain ellipsoid following material particles for the homogeneous flow case. (a) For the central domain of a vertical zone at any depth or the marginal domain on the FOT of a vertical zone. (b) For the marginal domain at $Z = 0.5$ of a vertical zone. (c) For the central domain of an inclined zone at any depth or the marginal domain on the FOT of an inclined zone. (d) For the marginal domain at $Z = 0.5$ of an inclined zone.

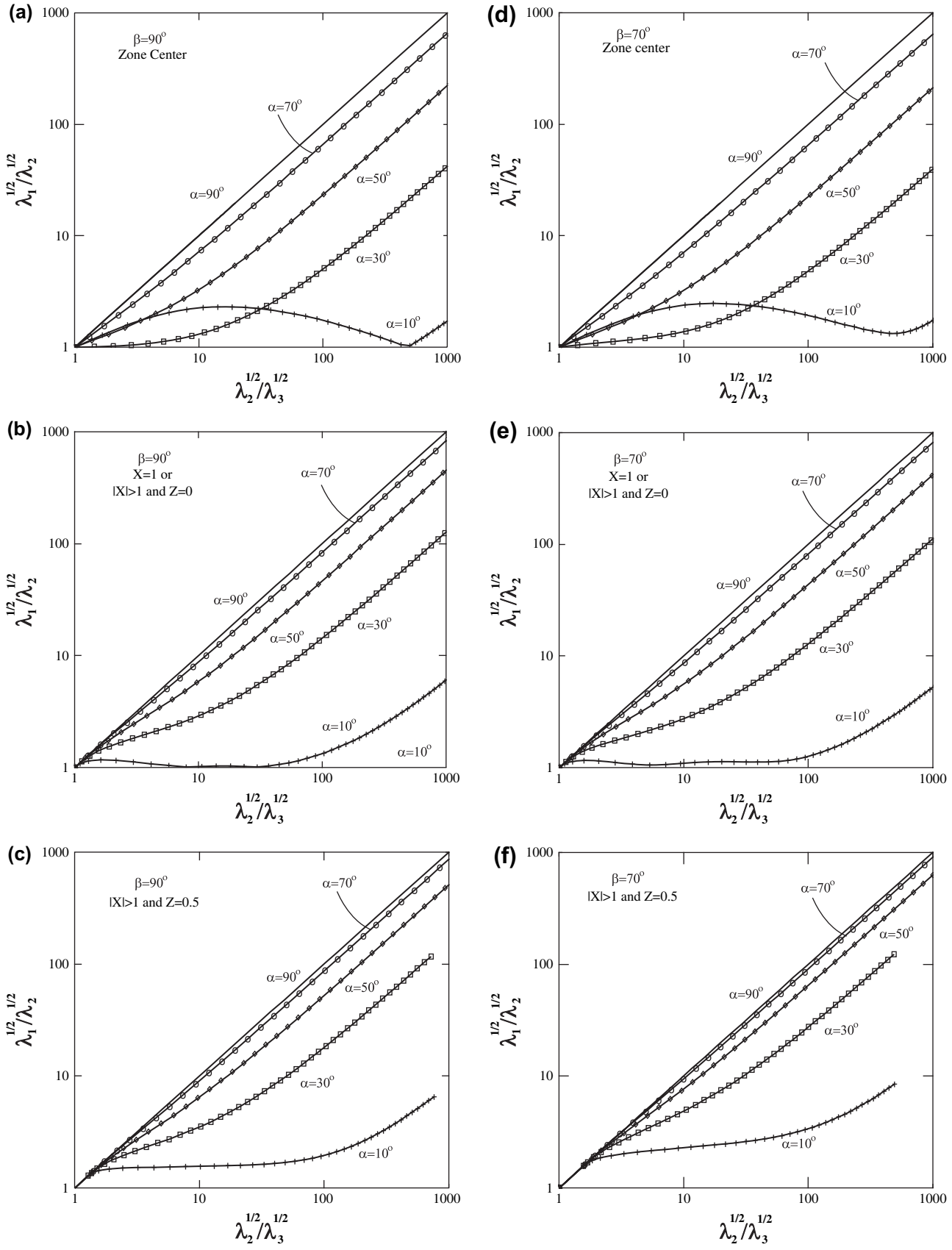

Fig. 6. Flinn diagrams showing evolution paths of the finite strain ellipsoid following material particles for the simple shear concentration case. See text for more discussion.

the central domain (center of the zone $X = 0$ or $|X| < 1$, Fig. 6a, b) of vertical transpressional zones with low convergence angles.

3.2. Strain intensity field

To measure the magnitude of the finite strain I adopt the strain intensity, S, defined by Ramsay and Huber (1983, pp. 201–202) as:

$$S = \sqrt{\left(\frac{\lambda_1^{1/2}}{\lambda_2^{1/2}} - 1\right)^2 + \left(\frac{\lambda_2^{1/2}}{\lambda_3^{1/2}} - 1\right)^2} \quad (10)$$

Fig. 7 presents the variation of S across the zone (only the range $0 \le x \le 1$ is shown because the zone is assumed to be symmetric about the central plane) for different convergence angles. All curves show rather simple profiles: a constant value in the central domain followed by an exponential decrease in the marginal domain for the homogeneous flow case, and more smooth variation for the simple shear concentration case. The profiles do not vary significantly with depth. The profiles are comparable to observations from natural shear zones interpreted to have undergone simple shear (e.g., Ramsay and Graham, 1970, Ramsay and Allison, 1979).

3.3. Variation in the orientations of the principal strain axes across the zone and with depth

Figs. 8–11 are lower hemisphere equal-area projection of the λ_1- and λ_3-axes across the model zones of various α- and β-values and at different depth levels. The left column of each figure is for the homogeneous flow case and the

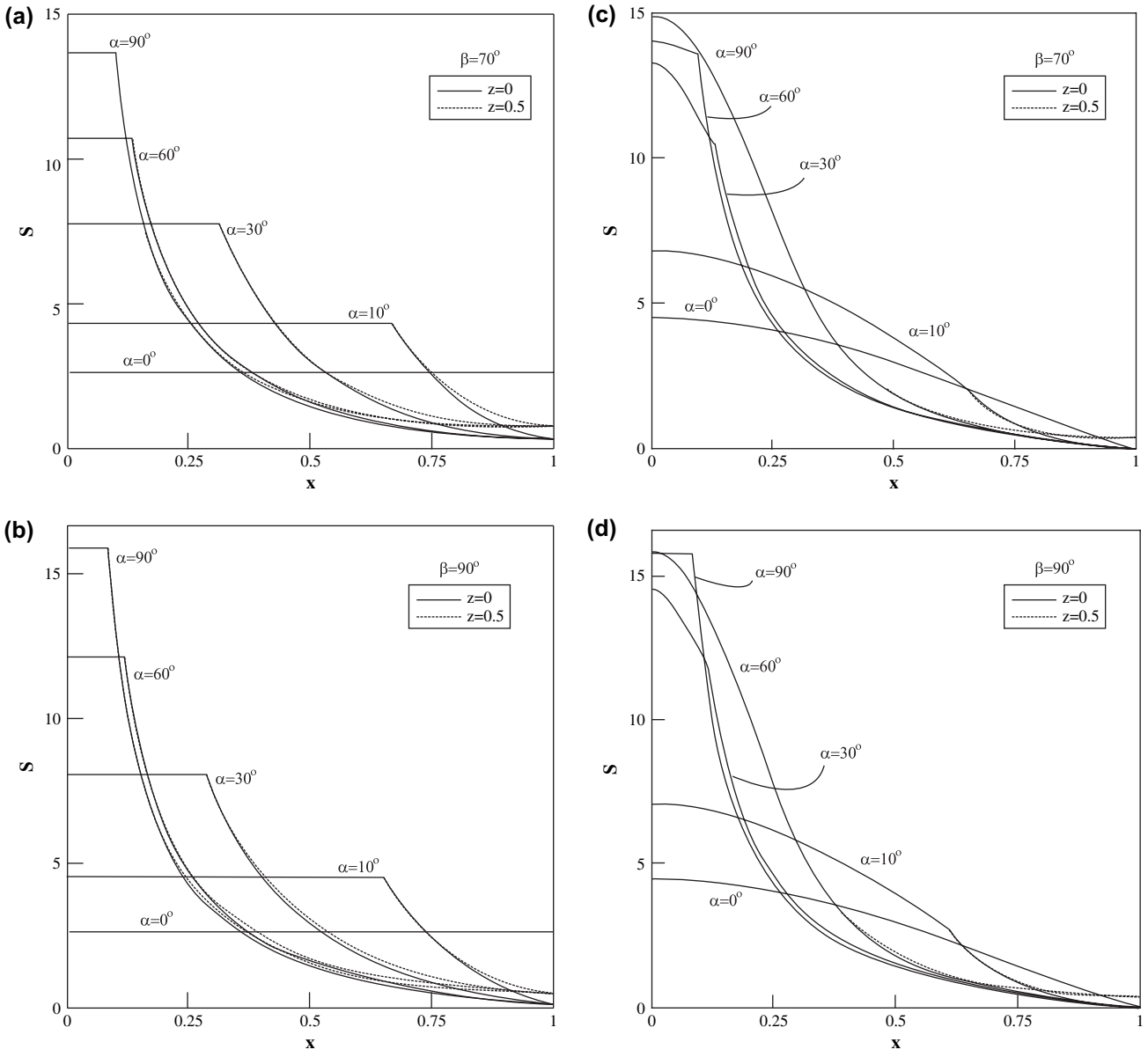

Fig. 7. Finite strain intensity (S) across the zone (because of symmetry, only variation over $0 \le x \le 1$ is shown) for different α-, β-, and z-values at the time $t = 10$ Myr, for the homogeneous flow case (a and b) and the simple shear concentration case (c and d).

right column for the simple shear concentration case. Different diagrams in each column are for different depths. For all cases, the strain geometry does not vary significantly with depth.

Fig. 8 is for a vertical ($\beta = 90°$) model zone with $\alpha = 10°$ at different depth levels. The coordinate axes and sense of shear of the zone are shown in Fig. 8e. The two sets of orientation trajectories for λ_1- and λ_3-axes in each stereonet of Fig. 8 and subsequent Figs. 9–11 correspond to the two sides ($-1 < x < 0$, and $0 < x < 1$, respectively) of the zone. On the FOT ($z = 0$) for both the homogeneous flow case (Fig. 8a) and the simple shear concentration case (Fig. 8f) or in the central domain of the homogeneous flow case (Fig. 8e), the finite strain axes are like those for the monoclinic Sanderson and Marchini transpression zone. The small table in Fig. 8e lists the strain magnitude (S) corresponding to each set of λ_1- and λ_3-plot. Both λ_1 and λ_3-axes plot on the horizontal plane, and at high strains ($S > 93$ for the current set of parameters) λ_1-axes are vertical (Fig. 8e). For both the homogeneous flow case and the simple shear concentration case, the λ_3-axes across the zone at any given level define a simple point maximum (Turner and Weiss, 1963, p. 58) close to the normal to the zone boundary (x-axis). As the center of the zone is approached (up the strain gradient, arrows in Fig. 8), the λ_3-axes approach the zone normal. For the simple shear concentration case, the λ_3-axes converge to the horizontal plane faster than the homogeneous flow case. The λ_1-axes across the zone exhibit a widespread for both cases. If lower strain ($S < 2.5$, empty dots in Fig. 8) points are neglected (fabrics may be too weak to observe at such low strains), the λ_1-axes across the entire zone ($-1 < x < 1$) approximately define a great circle girdle (Turner and Weiss, 1963, p. 58) subparallel to the zone boundary. In the simple shear concentration case (right column) the λ_1-axes converge to a great circle, as strain increases, faster than the homogeneous flow case.

Fig. 9 is for a vertical transpressional zone ($\beta = 90°$) with $\alpha = 30°$ at different depth levels. The coordinate system and sense of shear are the same as Fig. 8e. All statements made for Fig. 8 on the λ_3-axes are applicable, *en masse*, to this situation. The λ_1-axes, however, all pitch close to down dip on the $\lambda_1\lambda_2$ plane. If lower strain ($S < 2.5$) domains are neglected, the λ_1-axes practically define a vertical point maximum.

Fig. 10 is for an inclined model zone ($\beta = 70°$) with $\alpha = 10°$ at different depth levels. The coordinate axes and sense of shear are shown in Fig. 10e. The λ_3-axes define a simple point maximum close to the zone normal for both the homogeneous flow and the simple shear concentration cases. The λ_1-axes are widespread. In the central domain of the homogeneous flow case, the λ_1-axes lie close to parallelism with the zone boundary at high strains ($S > 17$, Fig. 10e). The small table in Fig. 10e lists the strain magnitude (S) corresponding to each orientation). In the marginal domains (Fig. 10a, b, c, d), the λ_1-axes define a great circle like girdle subparallel to the zone boundary if lower strain data are neglected. At extremely high strains ($S > 20$, stars), the λ_1-axes define a very good great circle girdle. For the simple shear concentration case (Fig. 10f, g, h, and i), the λ_1-axes converge to a great circle subparallel to the zone boundary faster than the homogeneous flow case as the center of the zone is approached (up the strain gradient, arrows in the figure).

Fig. 11 is for an inclined model zone ($\beta = 70°$) with $\alpha = 30°$ at different depth levels. The coordinate axes and sense of shear are shown in Fig. 11e. Again, the λ_3-axes define a simple point maximum close to the zone normal. The λ_1-axes also define a simple point maximum close to the dip line of the zone boundary if lower strain ($S < 2.5$) data are neglected. In the central domain of the homogeneous flow case, the λ_1-axes lie close to parallelism with the zone boundary at high strains ($S > 7.7$, Fig. 11e. The small table in Fig. 11e lists the strain magnitude (S) corresponding to each orientation.).

In summary, the modeling predicts that the $\lambda_1\lambda_2$ planes are always subparallel to the zone boundary regardless of the boundary conditions. The λ_1-axes cluster along the great circle subparallel to the zone boundary if lower strain cases are excluded. The λ_1-axes also tend to be widespread in pitch, defining a great circle like girdle at high strains, for model zones with low convergence angles. Simple shear concentration also strengthens girdle-like patterns. As the angle of convergence increases, the spread in the pitch of λ_1-axes shrinks and the λ_1-axes tend to define a point maximum parallel to the dip line of the zone boundary.

We can better understand the patterns of λ_1-axes as a function of α and β by introducing two other parameters: the ratio of the simple shear to pure shear in the zone (R) and the pitch of the shear direction on the shear plane (ϕ). Both are related to α and β:

$$R = \frac{\sqrt{\dot{\gamma}_{ss}^2 + \dot{\gamma}_{ds}^2}}{\dot{\varepsilon}} = \sqrt{\cot^2\alpha \csc^2\beta + \cot^2\beta} \tag{11}$$

$$\phi = \tan^{-1}\left(\frac{\dot{\gamma}_{ds}}{\dot{\gamma}_{ss}}\right) = \tan^{-1}(\tan\alpha \cos\beta) \tag{12}$$

In Fig. 12, isolines of R and ϕ are drawn on the α–β map. Where $\phi < 10°$, the high-strain zone is essentially strike slip, and where $\phi > 80°$ it is dip slip. Oblique-slip is $10° < \phi < 80°$. When R is high (>20), the strain geometry of the zone is essentially indistinguishable from that of zones of simple shear (Lin et al., 1998, 1999; Jiang and Williams, 1998). According to the present modeling, there are two possible λ_1-axis patterns. The λ_1-axes can define point-maxima-like patterns either parallel to the shear direction when $R > 20$, or parallel to the maximum principal stretch direction of the pure shear component (for transpressional high-strain zones, this is parallel to the dip line of the zone) at low R (Fig. 12). In a region roughly defined by $5° < \alpha < 25°$ (the range in α also depends weakly on β, see Fig. 12) and $\phi < 25°$ (Fig. 12), the λ_1-axes spread more widely forming girdle-like patterns with the girdle subparallel to the high-strain zone boundaries. Fig. 12 covers high-strain zones of all dip angles, but $\beta > 45°$ is appropriate for transpressional high-strain zones.

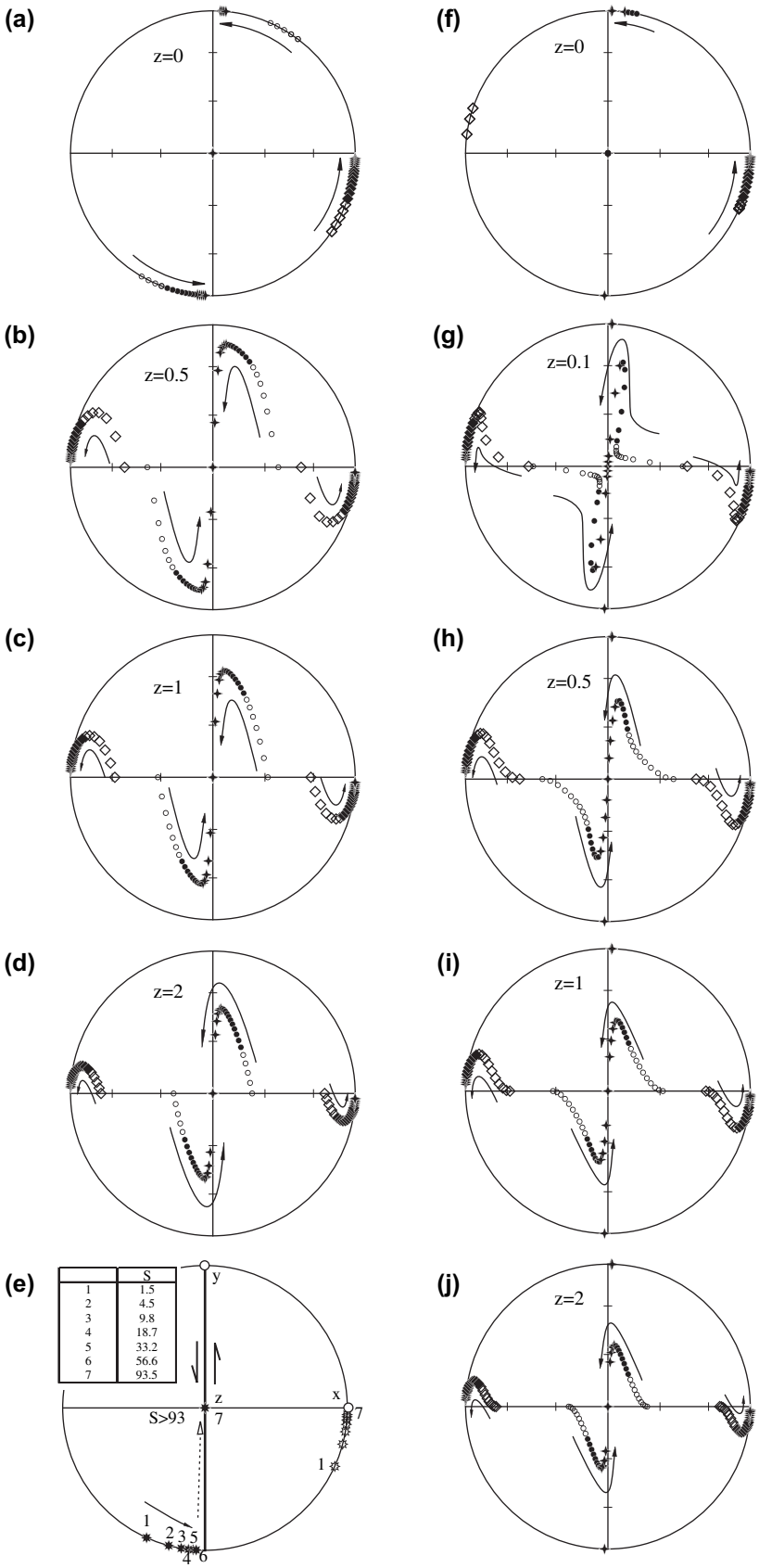

Fig. 8. Lower hemisphere equal-area projection of the λ_1-axes ($S < 2.5$, empty small circles; $2.5 < S < 20$, solid small circles; and $S > 20$, cross stars) and λ_3-axes ($S < 2.5$, empty squares; $2.5 < S < 20$, solid squares; and $S > 20$, cross stars) across the zone ($-1 \leq x \leq 1$) for a vertical zone with $\alpha = 10^\circ$ at different depths. The left column (a–e) is for the homogeneous flow case and the right column for the simple shear concentration case. See text for details.

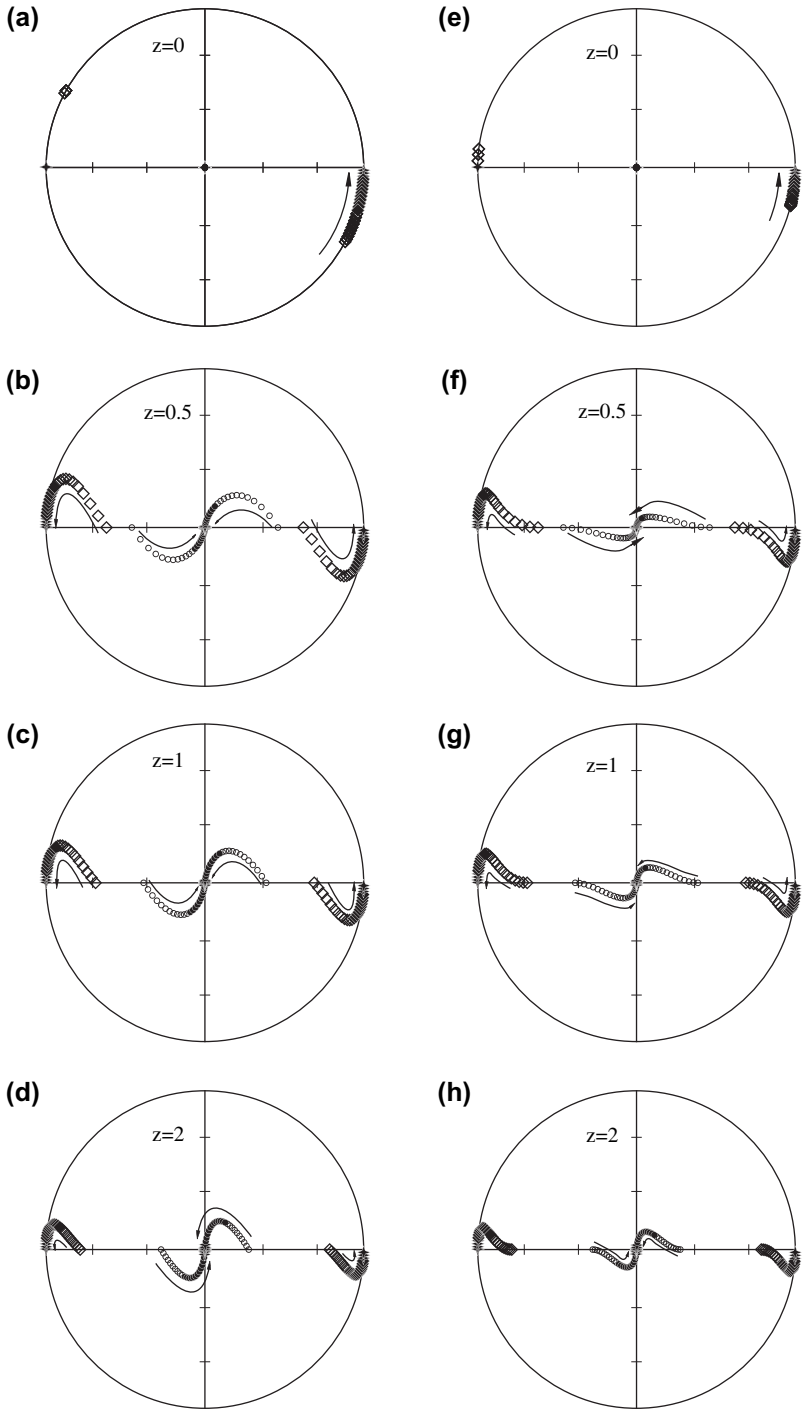

Fig. 9. Lower hemisphere equal-area projection of λ_1- and λ_3-axes for a vertical zone with $\alpha = 30°$. Symbols are the same as Fig. 8. The left column is for the homogeneous flow case and the right the simple shear concentration case. See text for details.

3.4. The stability of monoclinic ($\beta = 90°$) solutions: the problem of 'lineation switch'

The present modeling shows that as the zone approaches vertical ($\beta \rightarrow 90°$), if α is between 3° (equivalent to R = 20) and 19.5°, the λ_1-axes define girdle-like, rather than point-maximum-like patterns. This is different from the conclusion of Fossen and Tikoff (1993). Fossen and Tikoff (1993) show that for monoclinic ($\beta = 90°$) transpression, if $0° < \alpha < 19.5°$, the λ_1-axis is horizontal initially, but as the strain reaches certain value dependent on α, the λ_1-axis and the λ_2-axis swap and the λ_1-axis 'switches' to vertical thereafter. In terms of the evolution of the shape of the finite strain ellipsoid, at the instant of the swapping of the λ_1- and λ_2-axes, the strain ellipsoid is perfectly oblate and plots in the Flinn diagram on the abscissa (Figs. 5a, 6a). This phenomenon has been called

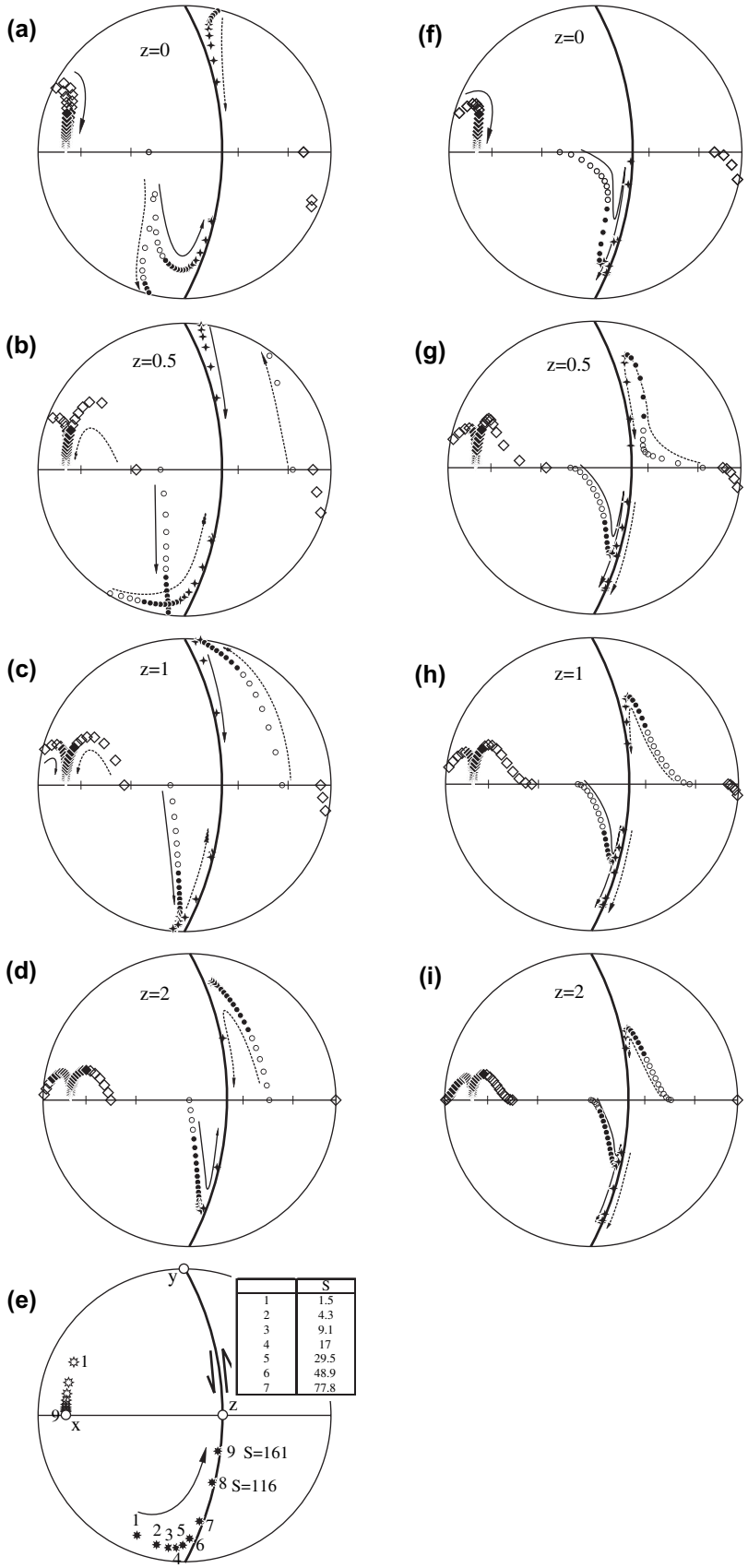

Fig. 10. Lower hemisphere equal-area projection of λ_1- and λ_3-axes for a zone with $\alpha = 10^\circ$ and $\beta = 70^\circ$. Symbols are the same as Fig. 8. The left column is for the homogeneous flow case and the right one for the simple shear concentration case. See text for details.

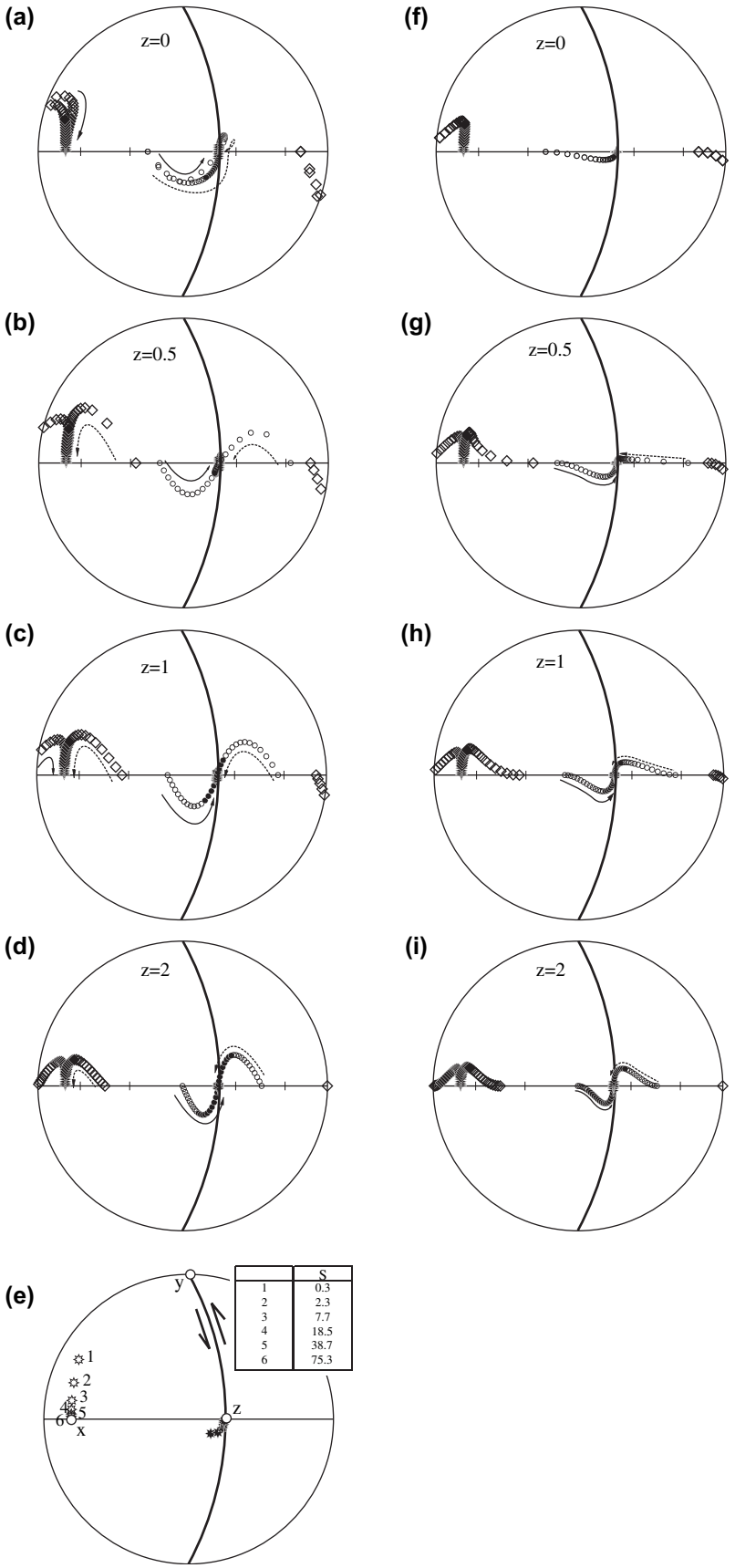

Fig. 11. Lower hemisphere equal-area projection of λ_1- and λ_3- axes similar to Fig. 8 for a zone with $\alpha = 30^\circ$ and $\beta = 70^\circ$. Symbols are the same as Fig. 8. The left column is for the homogeneous flow case and the right one for the simple shear concentration case. See text for details.

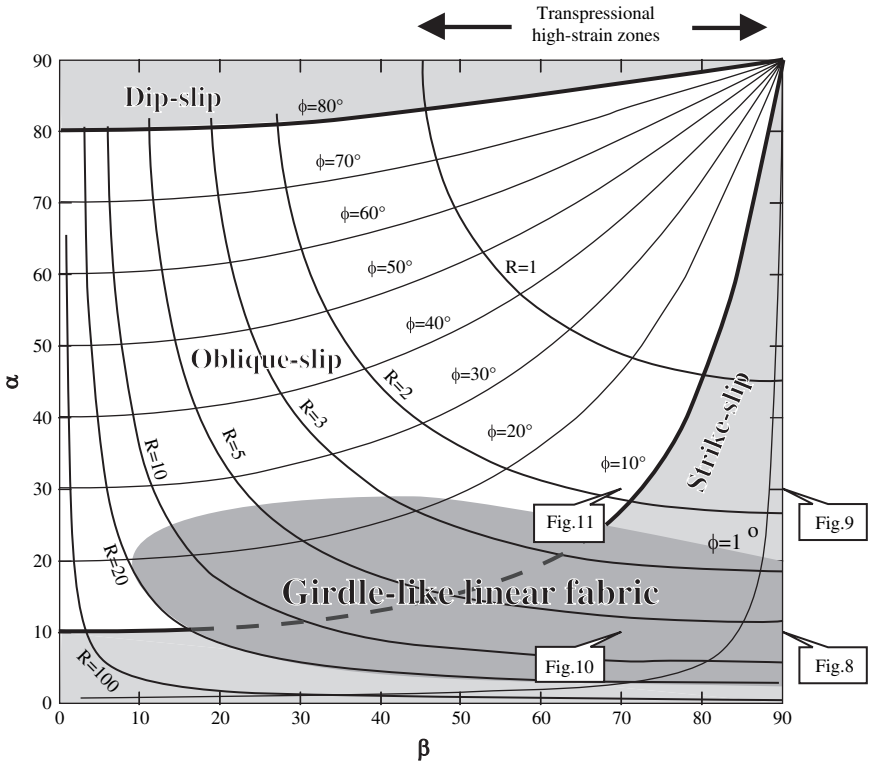

Fig. 12. The variation of λ_1-axis pattern on the $\alpha-\beta$ map for high-strain zones. Isolines of the simple shear to pure shear ratio (R) and the pitch of the shear direction (ϕ) are shown. The λ_1-axis pattern defines point maxima except in the domain ''girdle-like linear fabric''. In this domain the λ_1-axis tends to spread along a girdle subparallel to the zone boundary. Cases presented in the paper are shown.

the 'lineation switch' (e.g., Tikoff and Teyssier, 1994; Schulmann et al., 2003) and has been applied to interpret natural transpressional high-strain zones (e.g. Tikoff and Greene, 1997).

The monoclinic solution of Fossen and Tikoff (1993) is mathematically unstable. Consider the consequence of a slight deviation from the perfect monoclinic condition by giving a small perturbation in the pitch of the shear direction (ϕ) from exact zero. Fig. 13 shows that for any $\phi \neq 0°$, the λ_1-axis rotates progressively (Fig. 13c), rather than 'switches' instantaneously (Fig. 13b), from horizontal to vertical as strain increases. Therefore, an infinitesimally small deviation from the perfect condition of monoclinic symmetry (here equivalent to $\beta = 90°$) will render the lineation orientation to change progressively, in a continuous manner, from horizontal to vertical, rather than to switch instantaneously, in a discontinuous manner, from horizontal to vertical. Discontinuous lineation switch cannot be applied to natural transpressional zones because perfectly monoclinic transpression without even infinitesimal perturbations cannot exist in nature. The λ_1-axis pattern is predicted to be girdle-like for vertical transpressional zones with the convergence between 3° and 19.5°.

4. Discussion

The modeling results for both the homogeneous flow case and the simple shear concentration case are very similar, attesting to the stability of the mathematical solutions and suggesting that if simple shear concentration profiles different from Eqs. (7) were chosen for the modeling, similar results would be obtained.

4.1. Lineation patterns

The present model predicts simple patterns for the $\lambda_1\lambda_2$-plane across the zone. The prediction that the λ_1-axis can spread over a complete girdle at low angles of convergence is new. Previous monoclinic models predict point maxima λ_1-axis patterns and previous triclinic models can produce ''J-shaped'' or half girdle-like λ_1-axis patterns (Lin et al., 1998; Jiang and Williams, 1998). If the assumption is made, as in many studies (e.g. Ramsay and Graham, 1970; Tikoff and Greene, 1997; Jiang and Williams, 1998; Lin et al., 1998; Lin and Jiang, 2001), that the principal strain axes are directly related to the foliations and lineations, the model predictions are consistent with the observation that foliation patterns in transpressional zones are simply subparallel to the zone boundary. The present model provides an explanation for some stretching lineation patterns that spread over almost the entire girdle subparallel to the zone boundaries (Czeck and Hudleston, 2003; Xu et al., 2003; Bentley, 2004).

Can the girdle-like lineation pattern across a transpressional high-strain zone be explained by the variation in the pitch of the shear direction on the shear plane (e.g. Fig. 13c)? It can not, at least for reported natural examples. For this explanation to work, there must be domains between shallowly plunging

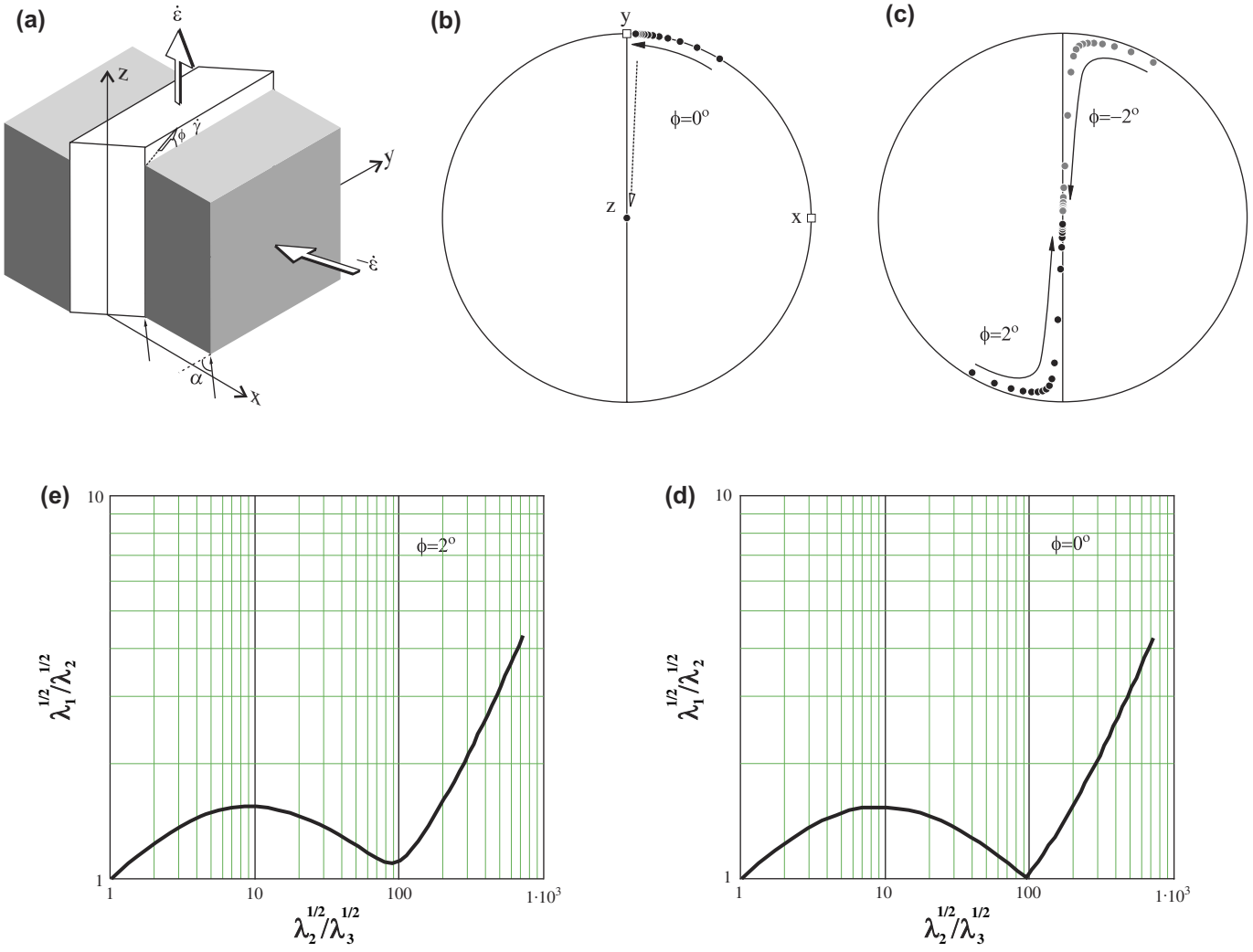

Fig. 13. The "lineation switch" based on monoclinic models is mathematically unstable. (a) Perfect monoclinic transpression deformation if $\varphi = 0°$. (b) "Lineation switch" only occurs for $\varphi = 0°$ and $0° < \alpha < 19.5°$. (c) For any infinitesimally small deviation from the perfect condition of $\varphi = 0°$, the lineation *rotates* progressively, rather than switches instantaneously toward vertical. The evolution of the finite strain ellipsoid shape for small φ (d) is similar to the case of $\varphi = 0°$ (e). But the ellipsoid never passes through the perfect oblate state when $\varphi \neq 0°$. See text for discussion.

lineations and steeply plunging lineation where the strain ellipsoid is close to perfectly oblate (Fig. 13d); these domains should be characterized by an absence of lineations. This has not been observed for any natural examples.

4.2. Complex strain geometry as a result of zone boundary migration

Although very simple, the present model can predict great geological complexity by varying the model variables.

First, a natural transpressional high-strain zone in its history of development may result from coalescing of many zones of strain concentration. Zone-normal convergence and zone boundary migration enable initially subparallel and separate shear zones to get closer and to combine into a single high-strain zone with complex strain geometry. The foliations in such an end product zone are expected to be subparallel to the orogenic boundary because, regardless of the boundary conditions, the foliations are subparallel to their hosting zone boundaries and the merging of individual zones only strengthens the parallelism between the foliations and the eventual zone boundaries. The lineations in the final combined zone may show great variability spreading on the great circle like girdle subparallel to the zone boundary. This is because lineations tend to cluster on the great circle girdle subparallel to foliations and the spread on the girdle reflects the variability in strain state and deformation history of different domains. These predicted strain patterns have been repeatedly observed in natural crustal scale shear zones including transpressional zones (Czeck and Hudleston, 2003; Xu et al., 2003; Bentley, 2004; Williams and Jiang, 2005; Williams et al., 2006).

Second, the present model assumes that the deforming zone is symmetric about its central plane. This is unlikely in nature. The migration of the two boundaries may be at different rates for a natural zone. This situation is easy to handle by the same approach as this paper but by treating the two halves separately. What is more challenging is that in a natural shear zone, strain localization occurring within the zone and tectonic

transposition due to ongoing non-coaxial progressive deformation may mingle the two halves, overprint and mix fabrics initially formed in the two halves of the zone. This would make it hard, if possible, for one to divide a shear zone into its two halves and to expect each half to have the lineation pattern spreading like a half girdle as predicted by Fig. 8. Instead, the general patterns would be that the foliations are subparallel to the zone boundaries and the lineations spread widely on a great circle like girdle parallel to the zone boundary (e.g., Czeck and Hudleston, 2003; Xu et al., 2003; Bentley, 2004). In some rare cases, the two halves of a shear zone can be identified. Lin (2005) reported a good example of such a shear zone. In the ENE trending Carrot River high-strain zone within the Carrot River greenstone belt, vertical boundary-parallel foliations are developed throughout the zone. In the NW half of the zone (NW subzone of Lin, 2005), the lineations define a half girdle pitching west and in the SE half (SE subzone of Lin, 2005) the lineations define another half girdle pitching east. Such lineation and foliation patterns are consistent with those predicted by the current model (e.g., Fig. 8).

Third, the thinning and the widening of the zone need not be exactly balanced. This would lead to transient variation in the strain rates. Since the modeling results are independent of the strain rates used, it is unnecessary to incorporate this effect.

Fourth, strain recorded in rocks is generally incomplete, discontinuous, and diachronic. In a continuous deformation the 'finite-strain clock' may be reset by recrystallization and other mechanisms continually (Means, 1981; Lister and Snoke, 1984). For instance, as the zone boundaries migrate, some domains may cease to deform transiently or permanently. It is also common during deformation that new rock material is added into the deforming system as veins, dykes, and plutons. If the effect of zone boundary migration is not considered, it may be possible to correlate different strain states with the deformation history of the zone (e.g. Tikoff and Greene, 1997). This practice becomes more problematic in a transpressional high-strain zone with migrating boundaries. Consider the following scenario. Suppose at time η since the onset of transpression a dyke was emplaced into the zone and started to record deformation. To keep the argument simple, let us assume that the flow is steady. The deformation recorded in the dyke is described by the position gradient tensor $\mathbf{F}(x, z, t\text{-}\eta)$. The finite deformation $\mathbf{F}(x, z, t\text{-}\eta)$ would depend on where and when the dyke was emplaced (x, z, and η). The strain geometry in the dyke may show great contrast with the surrounding rocks. Yet the dyke may be subparallel to the zone boundary as a result of tectonic transposition since its emplacement.

Finally, fabrics may not be simply related to strain. The assumption that the principal strain axes are directly related to the foliations and lineations is not always true and the model results should be applied where there is good reason to believe that the assumption is valid (Lin et al., 1998). Lineations defined by stretched passive clasts may track the major principal finite strain axes (Hossack, 1968; Czeck and Hudleston, 2003). But at high strains, an original single clast may be smeared out into many 'clasts' and the lineations defined by their long axes may not indicate the major principal axes of the total finite strain. If the clasts are rigid (Jeffery, 1922; Ježek et al., 1994, 1996) or deformable but more competent than the matrix (Eshelby, 1957, 1959; Bilby et al., 1975; Bilby and Kolbuszewski, 1977), then the lineation defined by their major axes are not, in general, the major principal finite strain axes either. Ježek et al. (1994, 1996) simulate the evolution of fabrics defined by rigid elements. Similar work on deformable elements is necessary to understand fabrics defined by them. Lineations defined by alignment of minerals, small-scale fold hingelines, etc. in transpressional zones may be understood by considering the rotation of material lines in transpressional deformation (Fossen et al., 1994; Passchier, 1997; Jiang and Williams, 1999). Only at very high strains, are these lineations subparallel to the major principal strain axes.

4.3. Relationship between bulk shortening and finite strain in the central domain

For shear zones with migrating boundaries, it is important to distinguish the 'thickness of the active zone' (T_a), which is assumed constant in this paper and probably does not vary significantly in nature, and the 'total thickness of rocks involved in the zone deformation throughout its history' (T_0). $T_a = 2D$ in the present model. T_0 is the unstrained thickness of the zone. For the model of this paper, a particle currently at the margin of the zone ($x = 1$) was initially in the wall rocks at X (Eq. (4c)) which leads to:

$$\frac{T_0}{T_a} = 1 + \dot{\varepsilon}t = 1 + \ln\left(\left.\frac{\partial z}{\partial Z}\right|_{x=0}\right) = 1 + \varepsilon \tag{13}$$

where ε is the natural logarithm stretch along the z-direction in the center of the zone. The average shortening across the zone, $\overline{\lambda}_x^{1/2}$, measured by the stretch (current length, 1, over initial length, X) is then:

$$\overline{\lambda}_x^{1/2} = \frac{1}{1+\varepsilon} = \frac{1}{1 + \ln\left(\lambda_z^{1/2}\big|_{x=0}\right)} \tag{14}$$

In the absence of detailed strain field data of a zone, Eq. (14) provides a rough estimate of the bulk shortening of the zone. The comparison of the estimate based on Eq. (14) with that based on a homogeneous transpression zone is shown in Fig. 14.

Many authors have used the kinematic vorticity number estimates and strain measurements to constrain the zone-normal shortening of crustal scale shear zones (e.g. Bailey et al., 2004; Giorgis and Tikoff, 2004). It is shown in the following that assuming the whole shear zone to be a homogeneous domain and the zone boundaries to be fixed to material planes can greatly overestimate the shortening across a crustal scale shear zone.

On the basis of vorticity and strain analysis, Bailey et al. (2004) proposed 70% and Giorgis and Tikoff (2004) proposed 92% shortening normal to the shear zones that they studied. Such a high component of pure shear poses significant strain compatibility problems (Hudleston, 1999; Williams et al.,

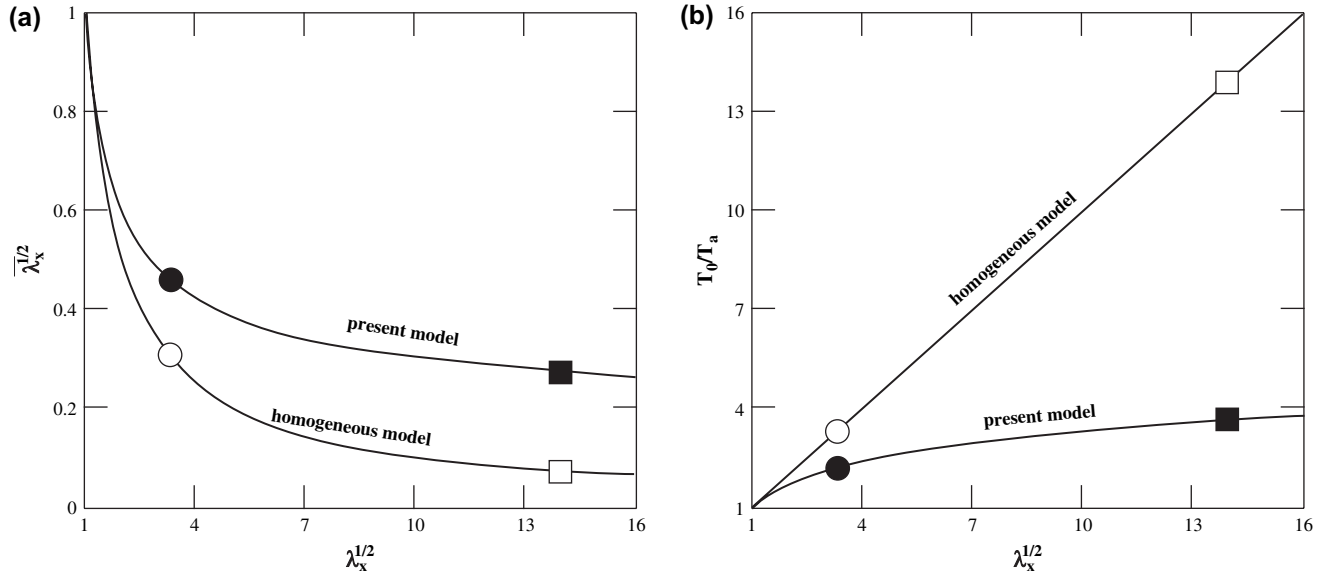

Fig. 14. (a) The model-based relationship between the stretch parallel to z-axis ($\lambda_z^{1/2}$) in the central domain of a transpressional high-strain zone and the *average* stretch across the zone in the direction normal to the zone boundaries (i.e. the x-direction, $\overline{\lambda}_x^{1/2}$). (b) The relationship between T_0/T_a and $\lambda_z^{1/2}$. The interpretation of Bailey et al. (2004) and Giorgis and Tikoff (2004) in terms of the Sanderson and Marchini model are plotted in white circles and squares, respectively. The interpretations based on the present model are plotted as solid circles and squares. See text for more details.

2006). Giorgis and Tikoff (2004) estimate that 92% across-zone shortening had occurred in the western Idaho shear zone (based on an estimate of the vertical stretch of 14). The present thickness of the western Idaho shear zone is around 4 km. In the context of a homogeneous transpressional zone with fixed boundaries, this implies that the zone was originally some 50 km thick. If one regards the vertical stretch of 14 as representing the strain in the central domain (not the entire zone) of the zone and allows its boundaries to migrate, the total thickness of rocks involved in the western Idaho shear zone deformation, measured in the undeformed state, is only around 15 km according to Eq. (13). Furthermore, in the current model, since thinning of the zone is offset by the migration of the zone boundaries to keep the zone thickness more or less constant, one may conclude that the thickness of the actively deforming zone of the western Idaho shear zone might have never been significantly more than 4 km in its entire history, although the zone has ''processed'' a much thicker package of rocks.

5. Conclusions

In order to sustain a transpressional motion (oblique convergence between plates and/or blocks), the boundaries of transpressional high-strain zones must migrate through rock material during the cause of deformation. In such high-strain zones, displacement continuity can be maintained at the active zone boundaries.

In high-strain zones with migrating boundaries, the strain geometry and kinematics are more complex than previous homogeneous models with fixed boundaries. The modeling predictions are as follows. The 'foliation' (assumed to be normal to the minimum principal strain axis) lies subparallel to the high-strain zone boundary regardless of the variation in model boundary conditions; the 'lineation' (assumed to be parallel to the maximum principal strain axes) clusters along a great circle girdle close to parallelism with the foliation. The 'lineation' spread may vary from point maxima to complete girdles depending on the obliquity of transpression and dip angle of the transpressional high-strain zone. These predicted fabric patterns have been documented in natural high-strain zones.

In natural monoclinic transpressional zones, lineations do not switch orientations by instantaneously swapping the maximum and intermediate principal strain axes. Instead, lineations change orientations by progressive rotation of the maximum principal strain axes.

The present model can predict great geological complexity by varying the model variables. A crustal scale transpressional high-strain zone may result from coalescence of many initially separate strain concentration zones; strain recorded in rocks is generally diachronic; continual tectonic transposition and strain localization take place during transpression. All this adds to the complexity of the strain geometry in a crustal scale transpressional high-strain zone.

For a shear zone with migrating boundaries, the thickness of its actively deforming part may not have fluctuated significantly in its history, although rocks now at the margins of the zone were initially farther away from the center of the shear zone.

Acknowledgements

My research on high-strain zones was supported by NSF (EAR0003315) and a Petroleum Research Fund during my tenure at the University of Maryland, College Park, an NSERC Discovery grant and the University of Western Ontario Academic Development Fund since I moved to Western. I also

thank Hefei University of Technology, China, for funding my research through a Professorship of Special Appointment. Review comments on earlier versions of the paper by W.P. Schellart, J. Ježek and P.J. Hudleston are appreciated.

Appendix A. Pure shear strain rate and boundary-normal velocity as functions of time in boundary-fixed zones

When the zone boundaries are fixed to material particles, the half thickness of the zone, D, decreases with time, and if the boundary-normal component of velocity relative to the center of the zone, V_n, is constant then:

$$D(t) = D_0 - V_n t \tag{A1}$$

where D_0 is the zone half thickness at $t = 0$.

The instantaneous pure shear strain rate, $\dot{\varepsilon}(t)$, is then:

$$\dot{\varepsilon}(t) = \frac{V_n}{D(t)} = \frac{V_n}{D_0 - V_n t} = \frac{V_n/D_0}{1 - (V_n/D_0)t} = \frac{\dot{\varepsilon}_0}{1 - \dot{\varepsilon}_0 t} \tag{A2}$$

where $\dot{\varepsilon}_0 = V_n/D_0$ is the pure shear strain rate at $t = 0$.

On the other hand, if the pure shear strain rate is constant (i.e., $\dot{\varepsilon} \equiv \dot{\varepsilon}_0$), then:

$$V_n(t) = -\frac{\mathrm{d}D}{\mathrm{d}t} = \dot{\varepsilon}_0 D \tag{A3}$$

Solving (A3), we obtain the relationship presented in the paper.

Appendix B. The relationships between strain rates and boundary velocity where the latter is not horizontal

Let us set up a coordinate system $x'y'z'$ (Fig. A1) where x'-axis is perpendicular to the strike of the zone, y'-axis parallel to the strike, and z'-axis is vertical and pointing upward. The total convergence velocity vector $\mathbf{v}$ (Fig. A1) expressed in this coordinate system has the following components:

$$\begin{aligned} v'_x &= -v\cos\delta\sin\alpha \\ v'_y &= v\cos\delta\cos\alpha \\ v'_z &= v\sin\delta \end{aligned} \tag{A4}$$

The base unit vectors ($\mathbf{i}$, $\mathbf{j}$, $\mathbf{k}$) of the coordinate system $x'y'z'$ and the base unit vectors ($\mathbf{e_1}$, $\mathbf{e_2}$, $\mathbf{e_3}$) of the high-strain zone coordinate system xyz (Fig. 3b and Fig. A1) are related by:

$$\begin{aligned} \mathbf{i} &= \sin\beta\mathbf{e}_1 + \cos\beta\mathbf{e}_3 \\ \mathbf{j} &= \mathbf{e}_2 \\ \mathbf{k} &= -\cos\beta\mathbf{e}_1 + \sin\beta\mathbf{e}_3 \end{aligned} \tag{A5}$$

Using (A5) and performing a vector transformation to express $\mathbf{v}$ in the high-strain zone coordinate system xyz, we have:

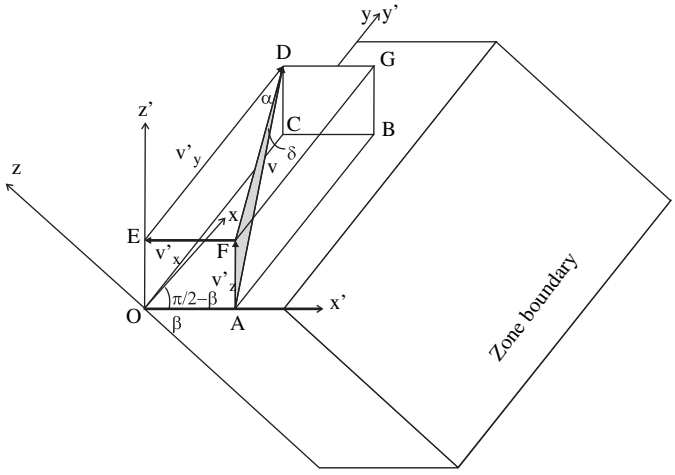

Fig. A1. Coordinate systems and zone orientation for deriving Eqs. (A7). The coordinate system xyz is the one used in the text (Fig. 3) where x-axis is perpendicular to the zone boundary, y-axis parallel to the zone strike, and the z-axis parallel to the dip line of the zone and pointing up. The coordinate system $x'y'z'$ is set up so that the $x'y'$ plane is horizontal, y'-axis is parallel to the y-axis, and the z'-axis is vertical and pointing up. Thus, OABC and DEFG are horizontal planes. The relative velocity V (AD) has a plunge angle δ ($\angle FDA$). The angle of convergence, α ($\angle EDF$), is the angle between the plunge direction of V and the strike of the zone. The velocity V can be easily expressed in $x'y'z'$ and then converted to corresponding expression in xyz.

$$\begin{aligned} v_x &= -v(\cos\delta\sin\alpha\sin\beta + \sin\delta\cos\beta) \\ v_y &= v\cos\delta\cos\alpha \\ v_z &= v(\cos\delta\sin\alpha\cos\beta + \sin\delta\sin\beta) \end{aligned} \tag{A6}$$

Normalizing Eqs. (A6) by D, we have:

$$\begin{aligned} \dot{\varepsilon}_v &= \tfrac{V}{D} \\ \dot{\varepsilon} &= \dot{\varepsilon}_v(\cos\delta\sin\alpha\sin\beta - \sin\delta\cos\beta) \\ \dot{\gamma}_{\mathrm{ss}} &= \dot{\varepsilon}_v\cos\delta\cos\alpha \\ \dot{\gamma}_{\mathrm{ds}} &= \dot{\varepsilon}_v(\cos\delta\sin\alpha\cos\beta + \sin\delta\sin\beta) \end{aligned} \tag{A7}$$

Appendix C. Derivation of equations for the homogeneous flow case

All expressions below are for normalized coordinates.

To obtain Eq. (4), one must solve the system of differential equations (Eq. (3)). It is sufficient to consider the situation of $x \geq 0$, for the situation of $x < 0$ can then be obtained by the symmetrical property of the solutions. Rewriting Eq. (3) for $x \geq 0$ only, we have:

$$\frac{\mathrm{d}x}{\mathrm{d}t} = \begin{cases} -\dot{\varepsilon}x, & 0 \leq x \leq 1 \\ -\dot{\varepsilon}, & x > 1 \end{cases} \quad \text{(a)}$$

$$\frac{\mathrm{d}y}{\mathrm{d}t} = \begin{cases} \dot{\gamma}_{\mathrm{ss}}x, & 0 \leq x \leq 1 \\ \dot{\gamma}_{\mathrm{ss}}, & x > 1 \end{cases} \quad \text{(b)} \tag{A8}$$

$$\frac{\mathrm{d}z}{\mathrm{d}t} = \begin{cases} \dot{\gamma}_{\mathrm{ds}}x + \dot{\varepsilon}z, & 0 \leq x \leq 1 \\ \dot{\gamma}_{\mathrm{ds}}, & x > 1 \end{cases} \quad \text{(c)}$$

In solving Eqs. (A8), there are three different cases to consider. The first is for material particles that were inside

the zone throughout deformation (i.e., $0 \le x \le 1$, note the distinction between Eulerian and Lagrangian coordinates). For this case the solution is given in Lin et al. (1998), and Jiang and Williams (1998). Written in the coordinate system used in this paper and generalized to include the other side of the zone, the solution is a set of three equations (Eqs. (6a-i), (6b-i), and (6c-i)) in the text (Eq. (1) is used to express the shear strain rates in terms of α, β, and $\dot{\varepsilon}$).

The second case is for material particles that were initially outside of the zone ($X > 1$) but were inside the zone eventually. This means that sufficient time since the onset of deformation has passed for the material particles to be transported into the deforming zone. The time, ξ, it takes for a particle at $X > 1$ to reach the zone boundary is:

$$\xi = \frac{X - 1}{\dot{\varepsilon}} \tag{A9}$$

because the boundary-normal velocity is $\dot{\varepsilon}$ (remember that normalized velocity is used) and the distance between the initial position of the particle and the zone boundary is $X - 1$. For a particle initially outside of the zone, if $t > \xi$, it will end up inside the zone. Once passing the zone boundary, the subsequent motion of the particle is identical to the particle that was at the zone boundary initially because the flow in the zone is steady. This means that to describe the motion of particles initially outside but finally inside the zone, we only need to replace the time term in Eqs. (6a-i), (6b-i), and (6c-i) with $t - \xi$, which represents the amount of time since the particle passed the zone boundary. This, after some algebraic manipulation and generalization to include the other half of the zone, leads to Eqs. (6a-ii), (6b-ii), and (6c-ii) in the text.

The third case is for material particles that were outside initially and remain outside of the zone throughout deformation. That is: $|X| > 1$ and $t \le \xi$. The motion of these particles is rigid translation described by Eqs. (6a-iii), (6b-iii), and (6c-iii) in the text.

Appendix D. Derivation of equations for the simple shear concentration case

In the event where there is localization of the simple shear component within the zone, both the strike-slip and dip-slip components of the simple shear are function of x and the velocity gradient tensor is:

$$L(x) = \begin{cases} \begin{pmatrix} -\dot{\varepsilon} & 0 & 0 \\ \dot{\gamma}_{ss}(x) & 0 & 0 \\ \dot{\gamma}_{ds}(x) & 0 & \dot{\varepsilon} \end{pmatrix}, & |x| \le 1 \\ \begin{pmatrix} 0 & 0 & 0 \\ 0 & 0 & 0 \\ 0 & 0 & 0 \end{pmatrix}, & |x| > 1 \end{cases} \tag{A10}$$

Rewriting this equation in a set of differential equations (for $x \ge 0$), we have:

$$\frac{dx}{dt} = \begin{cases} -\dot{\varepsilon}x, & 0 \le x \le 1 \\ -\dot{\varepsilon}, & x > 1 \end{cases} \quad \text{(a)}$$

$$d\frac{dy}{dt} = \begin{cases} \dot{\gamma}_{ss}(x)dx, & 0 \le x \le 1 \\ 0, & x > 1 \end{cases} \quad \text{with } \left.\frac{dy}{dt}\right|_{x>1} = \dot{\varepsilon}\cot\alpha \csc\beta \quad \text{(b)}$$

$$d\frac{dz}{dt} = \begin{cases} \dot{\gamma}_{ds}(x)dx + \dot{\varepsilon}\, dz, & 0 \le x \le 1 \\ 0, & x > 1 \end{cases} \quad \text{with } \left.\frac{dy}{dt}\right|_{x>1} = \dot{\varepsilon}\cot\beta \quad \text{(c)} \tag{A11}$$

The solutions to Eqs. (A11) are, after being generalized to include $x < 0$, Eq. (6) in the text.

References

Bailey, C.M., Francis, B.E., Fahrney, E.E., 2004. Strain and vorticity analysis of transpressional high-strain zones from the Virginia Piedmont, USA. In: Alsop, G., Holdsworth, R.E., McCaffrey, K.J.W., Hand, M. (Eds.), Flow Processes in Faults and Shear Zones. Geological Society Special Publication, vol. 224, pp. 249–264.

Ben-Avraham, Z., Nur, A., 1976. Slip rates and morphology of continental collision belts. Geology 4, 661–664.

Bentley, C., 2004. Rock fabric analysis of the Sierra Crest shear zone system, California: implications for crustal-scale transpressional shear zones. Unpublished M.Sc. thesis, University of Maryland.

Ben-Zion, Y., Sammis, C.G., 2003. Characterization of fault zones. Pure and Applied Geophysics 160, 677–715.

Berthé, D., Choukroune, P., Jegouzo, P., 1979. Orthogneiss, mylonite and non coaxial deformation of granite: the example of the South Armorican shear zone. Journal of Structural Geology 1, 31–42.

Bilby, B.A., Eshelby, J.D., Kundu, A.K., 1975. The change of shape of a viscous ellipsoidal region embedded in a slowly deforming matrix having a different viscosity. Tectonophysics 28, 265–274.

Bilby, B.A., Kolbuszewski, M.L., 1977. The finite deformation of an inhomogeneity in two-dimensional slow viscous incompressible flow. Proceedings of the Royal Society of London A 355, 335–353.

Bowman, D., King, G., Tapponnier, P., 2003. Slip partitioning by elastoplastic propagation of oblique slip at depth. Science 300, 1121–1123.

Czeck, D.M., Hudleston, P.J., 2003. Testing models for obliquely plunging lineations in transpression; a natural example and theoretical discussion. Journal of Structural Geology 25, 959–982.

DeMets, C., Gordon, R.G., Argus, D.F., Stein, S., 1990. Current plate motions. Geophysical Journal International 101, 425–478.

Dewey, J.F., Hempton, M.R., Kidd, W.S.F., Saroglu, F., Şengör, A.M.C., 1986. Shortening of continental lithosphere: the neotectonics of Eastern Anatolia – a young collision zone. In: Coward, M.P., Ries, A.C. (Eds.), Collision Tectonics. Geological Society Special Publication, vol. 19, pp. 3–36.

Dewey, J.F., Holdsworth, R.E., Strachan, R.A., 1998. Transpression and transtension zones. In: Holdsworth, R.E., Strachan, R.A., Dewey, J.F. (Eds.), Continental Transpressional and Transtensional Tectonics. Geological Society Special Publication, vol. 135, pp. 1–14.

Dutton, B.J., 1997. Finite strains in transpression zones with no boundary slip. Journal of Structural Geology 19, 1189–1200.

Elliott, D., 1972. Deformation paths in structural geology. Geological Society of America Bulletin 83, 2621–2638.

Eshelby, J.D., 1957. The determination of the elastic field of an ellipsoidal inclusion, and related problems. Proceedings of the Royal Society of London A 241, 376–396.

Eshelby, J.D., 1959. The elastic field outside an ellipsoidal inclusion. Proceedings of the Royal Society of London A 252, 561–569.

Fitch, T.J., 1972. Plate convergence, transcurrent faults, and internal deformation adjacent to Southeast Asia and the western Pacific. Journal of Geophysical Research 77, 4432–4460.

Fossen, H., Tikoff, B., 1993. The deformation matrix for simultaneous simple shearing, pure shearing, and volume change, and its application to

transpression/transtention tectonics. Journal of Structural Geology 15, 413–422.
Fossen, H., Tikoff, B., Teyssier, C., 1994. Strain modeling of transpressional and transtensional deformation. Norsk Geologisk Tidsskrift 74, 134–145.
Giorgis, S., Tikoff, B., 2004. Constraints on kinematics and strain from feldspar porphyroclast populations. In: Alsop, G., Holdsworth, R.E., McCaffrey, K.J.W., Hand, M. (Eds.), Flow Processes in Faults and Shear Zones. Geological Society of London Special Publication, vol. 224, pp. 265–285.
Harland, W.B., 1971. Tectonic transpression in Caledonian Spitsbergen. Geological Magazine 108, 27–42.
Holdsworth, R.E., Butler, C.A., Roberts, A.M., 1997. The recognition of reactivation during continental deformation. Journal of Geological Society of London 154, 73–78.
Hossack, J.R., 1968. Pebble deformation and thrusting in the Bygdin area (S. Norway). Tectonophysics 5, 315–339.
Hudleston, P.J., 1999. Strain compatibility and shear zones: is there a problem? Journal of Structural Geology 21, 923–932.
Jaeger, J.C., 1964. Elasticity, Fracture and Flow. John Wiley & Sons, New York.
Jeffery, G.B., 1922. The motion of ellipsoidal particles immersed in a viscous fluid. Proceedings of the Royal Society of London A 102, 161–179.
Ježek, J., Melka, R., Schulmann, K., Venera, Z., 1994. The behavior of rigid triaxial particles in viscous flows – modeling of fabric evolution in a multiparticle system. Tectonophysics 229, 165–180.
Ježek, J., Schulmann, K., Segeth, K., 1996. Fabric evolution of rigid inclusions during mixed coaxial and simple shear flows. Tectonophysics 257, 203–221.
Jiang, D., Lin, S., Williams, P.F., 2001. Deformation path in high-strain zones, with reference to slip partitioning in transpressional plate-boundary regions. Journal of Structural Geology 23, 991–1005.
Jiang, D., Williams, P.F., 1998. High-strain zones: a unified model. Journal of Structural Geology 20, 1105–1120.
Jiang, D., Williams, P.F., 1999. When do dragfolds not develop into sheath folds in shear zones? Journal of Structural Geology 21, 577–583.
Jones, C.H., Wesnousky, S.G., 1992. Variations in strength and slip rate along the San Andreas fault system. Science 256, 83–86.
Jones, R.R., Holdsworth, R.E., Baily, W., 1997. Lateral extrusion in transpression zones. Journal of Structural Geology 19, 1201–1217.
Jones, R.R., Tanner, P.W.G., 1995. Strain partitioning in transpression zones. Journal of Structural Geology 17, 1125–1137.
Jones, R.R., Holdsworth, R.E., Clegg, P., McCaffrey, K., Tavarnelli, E., 2004. Inclined transpression. Journal of Structural Geology 26, 1531–1548.
Lin, S., 2005. Synchronous vertical and horizontal tectonism in the Neoarchean: Kinematic evidence from a synclinial keel in the northwestern Superior craton, Canada. Precambrian Research 139, 181–194.
Lin, S., Jiang, D., 2001. Using along-strike variation in strain and kinematics to define the movement direction of curved transpressional shear zones: an example from the northwestern Superior Province, Manitoba. Geology 29, 767–770.
Lin, S., Jiang, D., Williams, P.F., 1998. Transpression (or transtension) zones of triclinic symmetry: natural example and theoretical modeling. In: Holdsworth, R.E., Strachan, R., Dewey, J.F. (Eds.), Continental Transpressional and Transtensional Tectonics. Geological Society Special Publication, vol. 135, pp. 41–57.
Lin, S., Jiang, D., Williams, P.F., 1999. Discussion on transpression and transtension zones. Journal of Geological Society of London 156, 1045–1048.
Lister, G.S., Snoke, A.W., 1984. S–C mylonites. Journal of Structural Geology 6, 617–638.
Lister, G.S., Williams, P.F., 1983. The partitioning of deformation in flowing rock masses. Tectonophysics 92, 1–33.
Little, T.A., 2004. Transpressive ductile flow and oblique ramping of lower crust in a two-sided orogen: Insight from quartz grain-shape fabrics near the Alpine fault, New Zealand. Tectonics 23, TC2013, doi:10.1029/2002TC001456.
Mattauer, M., Faure, M., Malavieille, J., 1981. Transverse lineation and large-scale structures related to alpine obduction in Corsica. Journal of Structural Geology 3, 401–409.
McCaffrey, R., 1992. Oblique plate convergence, slip vectors, and forearc deformation. Journal Geophysical Research 97, 8905–8915.
McCaffrey, R., 1994. Global variability in subduction thrust zone – forearc systems. Pure and Applied Geophysics 142, 173–224.
McKenzie, D., Jackson, J., 1983. The relationship between strain rates, crustal thickening, palaeomagnetism, finite strain and fault movements within a deforming zone. Earth and Planetary Science Letters 65, 182–202.
Means, W.D., 1981. Concept of steady state foliation. Tectonophysics 96, 331–352.
Means, W.D., 1995. Shear zones and rock history. Tectonophysics 247, 157–160.
MathCad® 11: User's Guide, 2002. Mathsoft Engineering & Education, Inc., Cambridge, MA.
Passchier, C.W., 1997. The fabric attractor. Journal of Structural Geology 19, 113–127.
Ramberg, H., 1975. Particle paths, displacement and progressive strain applicable to rocks. Tectonophysics 28 (1–37), 1975.
Ramsay, J.G., Allison, I., 1979. Structural anslysis of shear zones in an alpinised Hercynian granite. Schweizerische Mineralogische und Petrographische Mitteilurgen 59, 251–279.
Ramsay, J.G., Graham, R.H., 1970. Strain variation in shear belts. Canadian Journal of Earth Sciences 7, 786–813.
Ramsay, J.G., Huber, M.I., 1983. The Techniques of Modern Structural Geology. In: Strain Analysis, vol. 1. Academic Press, San Diego.
Robin, P.-Y.F., Cruden, A.R., 1994. Strain and vorticity patterns in ideally ductile transpressional zones. Journal of Structural Geology 16, 447–466.
Royden, L., 1996. Coupling and decoupling of crust and mantle in convergent orogens: Implications for strain partitioning in the crust. Journal of Geophysical Research 101, 17,679–17,705.
Sanderson, D.J., Marchini, W.R.D., 1984. Transpression. Journal of Structural Geology 6, 449–458.
Schulmann, K., Thompson, A.B., Lexa, O., Ježek, J., 2003. Strain distribution and fabric development modeled in active and ancient transpressive zones. Journal of Geophysical Research 108 (B1), 2023, doi:10.1029/2001JB000632.
Schwerdtner, W.M., 1989. The solid-body tilt of deformed paleohorizontal planes: application to Archean transpression zones, Southern Canadian Shield. Journal of Structural Geology 11, 1021–1027.
Spencer, A.J.M., 1980. Continuum Mechanics. Longman, New York.
Tikoff, B., Fossen, H., 1993. Simultaneous pure and simple shear: the unifying deformation matrix. Tectonophysics 217, 267–283.
Tikoff, B., Greene, D., 1997. Stretching lineations in transpressional shear zones. Journal of Structural Geology 19, 29–40.
Tikoff, B., Teyssier, C., 1994. Strain modeling of displacement field partitioning in transpressional orogens. Journal of Structural Geology 16, 1575–1588.
Truesdell, C.A., Toupin, R.A., 1960. The classic field theory. In: Flügge, S. (Ed.), Encyclopedia of Physics. Principles of Classical Mechanics and Field Theory, vol. II. Springer-Verlag, Berlin, pp. 226–793.
Tommasi, A., Vauchez, A., 2001. Continental rifting parallel to ancient collisional belts: an effect of the mechanical anisotropy of the lithospheric mantle. Earth and Planetary Science Letters 185, 199–210.
Turner, F.J., Weiss, L.E., 1963. Structural Analysis of Metamorphic Tectonites. McGraw-Hill, New York.
White, S.H., Burrows, S.E., Carreras, J., Shaw, N.D., Humphreys, F.J., 1980. On mylonites in ductile shear zones. Journal of Structural Geology 2, 175–187.
Williams, P.F., Jiang, D., 2005. An investigation of lower crustal deformation: evidence for channel flow and its implications for tectonics and structural studies. Journal of Structural Geology 27, 1486–1504.
Williams, P.F., Jiang, D., Lin, S., 2006. Interpretation of deformation fabrics of infrastructure zone rocks in the context of channel flow and other tectonic models. In: Law, R.D., Searle, M., Godin, L. (Eds.), Channel Flow, Ductile Extrusion and Exhumation of Lower-mid Crust in Continental Collision Zones. Geological Society Special Publication, vol. 268, pp. 221–235.
Xu, X.-W., Ma, T.-L., Sun, L.-Q., Cai, X.-P., 2003. Characteristics and dynamic origin of the large-scale Jiaoluotage ductile compressional zone in the eastern Tianshan Mountains, China. Journal of Structural Geology 25, 1901–1915.